T / IB 00 / 00794
21.07.00
#2
22/2

Eur päisches Patentamt | Eur pean Patent Office | Office européen des brevets

REC'D 24 JUL 2000
WIPO PCT

Bescheinigung | Certificate | Attestation

4

Die angehefteten Unterlagen stimmen mit der ursprünglich eingereichten Fassung der auf dem nächsten Blatt bezeichneten europäischen Patentanmeldung überein.

The attached documents are exact copies of the European patent application described on the following page, as originally filed.

Les documents fixés à cette attestation sont conformes à la version initialement déposée de la demande de brevet européen spécifiée à la page suivante.

Patentanmeldung Nr. | Patent application No. | Demande de brevet n°

99111446.3

PRIORITY DOCUMENT

SUBMITTED OR TRANSMITTED IN COMPLIANCE WITH RULE 17.1(a) OR (b)

Der Präsident des Europäischen Patentamts;
Im Auftrag

For the President of the European Patent Office

Le Président de l'Office européen des brevets
p.o.

I.L.C. HATTEN-HECKMAN

DEN HAAG, DEN
THE HAGUE,
LA HAYE, LE 13/07/00

Eur päisches Patentamt | Eur pean Patent Office | Office eur péen des brevets

Blatt 2 der Bescheinigung
Sheet 2 of the certificate
Page 2 de l'attestation

Anmeldung Nr.:
Application no.:
Demande n°: 99111446.3

Anmeldetag:
Date of filing:
Date de dépôt: 11/06/99

Anmelder:
Applicant(s):
Demandeur(s):
HOLTRONIC TECHNOLOGIES LIMITED
London EC4A 1NH
UNITED KINGDOM

Bezeichnung der Erfindung:
Title of the invention:
Titre de l'invention:
Method and apparatus for recording a hologram from a mask pattern by the use of total internal reflection holography

In Anspruch genommene Priorität(en) / Priority(ies) claimed / Priorité(s) revendiquée(s)

Staat: State: Pays:	Tag: Date: Date:	Aktenzeichen: File no. Numéro de dépôt:

Internationale Patentklassifikation:
International Patent classification:
Classification internationale des brevets:
/

Am Anmeldetag benannte Vertragstaaten:
Contracting states designated at date of filing: AT/BE/CH/CY/DE/DK/ES/FI/FR/GB/GR/IE/IT/LI/LU/MC/NL/PT/SE
Etats contractants désignés lors du depôt:

Bemerkungen:
Remarks:
Remarques:

Method and apparatus for recording a hologram from a mask pattern by the use of total internal reflection holography

The present invention relates to a total internal reflection holographic apparatus and a method of forming a hologram and reconstructing an image therefrom.

The principles of total internal reflection (TIR) holography have been described already in US 4,857,425. Since then many efforts have been made to make use of TIR holography in the microelectronics industries. Prior art references are e.g. US 4,917,497, US 4,966,428, 5,187,372, US 5,640,257 and European application no. 98300188 whose contents are herewith incorporated by reference.

Frosch et al. (US 3,796,46)recorded TIR holograms of mask pattern using photographic emulsion, i.e. grains of silver halide dispersed in a gelatin film, as the holographic recording material. Such a material records information by modulating the bulk properties of the material (either absorption or refractive index and is referred to hereinafter as a "volume recording material".

Normally in TIR holography the three recording beams (object beam, incident reference beam and totally internally reflected beam) give rise to three holograms in the recording material. Frosch et al. used object and reference beams whose planes of polarisation were orientated such that only one hologram is formed (either that formed by interference of the object beam with the incident reference beam or that formed by the interference of the object beam with the reflected reference beam) for the purpose of avoiding the (perceived) problem of loss of resolution due to shrinkage of the emulsion between recording and replay. According to Frosch et al., when both of the aforementioned holograms are present,

shrinkage of the emulsion causes the images generated by the two holograms of Frosch et al. to shift relative to each other, and this degrades the resolution.

However, the present inventors have found that the contention of Frosch et al., namely that shrinkage causes a relative shift of the two images reconstructed from the two holograms, is not true. In fact, shrinkage of the emulsion does not cause either of the images to shift and thus there is no relative shift of the two. Since 1974, when US 3,796,476 was published, no subsequent prior art on TIR holography directed at high resolution lithography has employed the polarisation scheme proposed by Frosch et al.

It is to be noted that Frosch et al. is directed at recording the hologram in a thick photosensitive emulsion having a layer thickness much greater than the length of the light used. Although Frosch et al. proposed to use TIR holography instead of then other known photolithographic methods, the disclosure of Frosch did not attract much attention and, as far as the present inventors knows, Frosch's method has never been employed industrially. The reason for this is as explained above: for volume holography, it did not offer any useful purpose.

The overwhelming part of the literature relating to the application of TIR holography to microlithography therefore concerns volume holography. In particular, the holograms are recorded in photopolymer materials manufactured by DuPont Nemours. With this material the pattern in the mask is recorded as a modulation of the refractive index in a layer of $\approx$ 10 µm thickness. In contrast thereto, surface-relief holography records the mask pattern information as a modulation of layer thickness.

In 1988 Ross et al. reported about recording TIR holograms of mask patterns using a wavelength of 458 nm, S-polarisation (i.e. electric field vector perpendicular to the plane of incidence of the reference beam at the recording layer) for the object and reference beams and photoresist as the holographic recording material. They used an argon-ion laser operating at 458 nm as the light source. They were able to obtain hologram efficiencies of only ~ 5 % which they partly attributed to the problem of obtaining deep surface-relief structures in the photoresist because of the intensity distribution of the 3 interfering beams in the photoresist (object beam, incident reference beam and reflected reference beam) and the development process which preferentially etches the high intensity regions.

An approach for achieving higher resolution from TIR holographic lithography is to reduce the wavelength of the light source for recording and replay from the commonly used value of 364 nm for instance, a value of 248 nm. Unfortunately, however no volume holographic recording material is available for such a wavelength.

It is an object of the present invention to provide an improved method and an improved total internal reflection (TIR) hologram apparatus for forming a hologram and reconstructing an image therefrom. In particular, it is an object to provide better resolution so that still smaller features can be recorded in a hologram and subsequently be reproduced therefrom. A further object is to

According to the invention there is provided a method according to the pre-characterizing part of claim 1 wherein a photoresist is employed as the holographic recording medium and the planes of polarisation are arranged of the object and reference beams incident on the holographic recording medium

such that their polarisation vectors are substantially mutually orthogonal in the holographic recording medium and such that the polarisation vectors of the incident and totally internally reflected reference beams are substantially orthogonal.

Advantageously, the plane of polarisation of the object beam is at 45° to the plane of incidence of the reference beam at the holographic recording layer. According to a preferred embodiment the object beam illuminates the mask at an off-axis angle i.e. not normal to the mask. Preferably only the transmission hologram is recorded in the holographic recording layer. Surprisingly, the best results can be obtained when only the transmission is recorded.

Advantageously, the photoresist material is selected such that its thickness (d) and absorption (a) meet the condition $a * d < 1$. The photoresist can be selected such that its contrast described by its gamma-value satisfies the condition $\gamma < 3$. Advantageously, photoresist is selected such that its resolution described by the smallest period of grating that can be optically recorded in the material is with a modulation depth $(d_{max} - d_{min})/ (d_{max} - d_{min}) > 25\%$ satisfies the condition $\Lambda < 200$ nm.

It is preferred that the laser light used has a wavelength of below 300nm, and preferably a wavelength between 150 and 260 nm. It has been found by the inventor that the polarisation angles are selected according to the refractive index of the photoresist.

Advantageously, a combination of polarisation angles of between 37 to 44°, preferably 39° for the reference beam and --43 to -47°, preferably -45° for the object beam with respect to the plane of incidence is applied. Further, it is

advantageous that the intensity of the reference beam exceeds that of the object beam, preferably by a factor 2, and preferably is 4 : 1. It has further been found that the best results can be obtained if the thickness of the photoresist layer is less than 500 nm, preferably between 100 and 300 nm and most preferably between 200 and 300 nm.

For a better long-term stability of the hologram it is further advisable when the image recorded in the photoresist as surface relief hologram is transferred into the substrate material by an etching process, e.g. plasma etching.

Although the hologram can be formed in a single exposure, preferably beams of a restricted cross-section are used and the hologram formed by a scan-and-step operation. The inventive process is particularly useful for transferring features of less than 1 µm, preferably less than 0.5 µm, from a mask into a hologram for use in microlithography.

The present invention relates also to a Total internal reflection holographic recording apparatus for recording a hologram from a mask, comprising

- an optical coupling element for receiving a substrate on a first face;
- a substrate bearing a holographic recording medium, the substrate being in optical contact with said first face of the optical coupling element,
- at least one light source for generating a light beam;
- optical means for generating a collimated light beam of a selected cross-section;
- means, e.g. a beam-splitter, prism or the like, for generating two coherent light beams, a reference light beam and an object light beam;
- means for directing the reference light beam at a second face of the coupling element such that it illuminates the

interface between the first face and the ambient medium or the interface between a substrate in optical contact with said first face and the ambient medium at an angle greater than the critical angle;

- means for directing the object light beam at the first face of the coupling element such that it is aligned with the reference beam in the plane of the holographic recording medium on the substrate in contact with the first face;

characterized in that

- the holographic recording medium is a photoresist; and
- means are provided for arranging the planes of polarisation of the object and reference beams incident on the holographic recording medium such that their polarisation vectors are substantially mutually orthogonal in the holographic recording medium and such that the polarisation vectors of the incident and totally internally reflected reference beams are substantially orthogonal. Further advantageous features are defined in the sub-claims.

The coupling element is e.g. a prism or a grating on a transparent plate or glass substrate as described in the co-pending European application no. EP 98300188 (published under no. EP 0 930 549). The coupling element disclosed in EP 0 930 549 is a glass substrate having a periodic grating structure on the first surface whose period, in relation to the incident angle and wavelength of the light and the refractive index of the plate material is such that only a zeroth and one first order beams of the light being incident on the first surface at a predetermined incident angle are transmitted into the plate and that the transmitted first diffraction order is essentially totally reflected at the second surface/air interface. Thus, the grating can behave like a prism in a TIR holographic process.

Advantageously the apparatus comprises means for measuring the gap between the holographic recording layer and the mask preferably at the centre of the scanning illumination beam, and means for adjusting the separation between the holographic recording layer and the mask.

For a more complete understanding of the present invention, reference is now made to the figures, like numerals being used for like and corresponding parts of the various drawings.

Fig.1 is a schematic view of a total internal reflection (TIR) holographic recording apparatus comprising a scanning stage for scanning an illumination beam in x and y direction (only x dimension shown);

Fig. 2 a view of the scanning stage from above;

Fig.3 the inventive TIR holographic recording system

Figure 1 shows a known TIR holographic system for forming an a hologram from a mask pattern. It usually comprises a prism 11 or alternatively a grating onto which a substrate 13 bearing a holographic recording layer 15 is index-matched by means of an appropriate matching fluid. The matching fluid is applied between prism 11 and substrate 13 and exhibits the same refractive index as the prism 11 and substrate material so that a light beam which passes from the prism 11 into the substrate 13 preferably is not reflected at the prism/substrate interface.

For forming a hologram two light beams are necessary, an object beam 17 and a reference beam 19. The object and reference beams 17,19 are coherent light beams which are usually derived from the same laser light source. The

normally narrow laser light beam is first preferably expanded and collimated by an expansion and collimating optics 21 to a beam of a diameter of about 15 to 20 mm by a known optical expansion means. Thereafter the expanded and collimated beam is directed by a mirror 23 towards a xy scanning stage 25. The two-axes xy scanning stage serves for deflecting the collimated light beam 27 such that the beam can traverse in a raster pattern essentially the entire prism face onto which the substrate 13 bearing the recording medium 15 is arranged. For this purpose the scanning stage 23 comprises a first mirror 29 on a first carriage 31 movable in the x direction which deflects the light beam to a second mirror 33 on a second stage 35 moveable in the x direction that is also mounted to the first carriage. This second mirror 35 deflects the beam onto further large mirrors 37,39 such that the light beam enters the prism 11 through the hypotenuse face 41 and arrives at the substrate bearing face of the prism at an angle which is greater than the critical angle. For, the orientation of the stage system it is preferable that the beam be scanned in the x direction and stepped in the y direction (it also allows the beam to be scanned in the y direction and stepped in the x direction, though this is not desirable because of mechanical wear to the first stage).

The mirror 37 is semi-transparent and functions as beam splitter for generating the object beam 17. The object beam 17 is directed to mirror 43 which deflects the beam 17 towards the substrate 13 at normal incidence.

For forming the hologram a mask 45 containing a mask pattern 47 is placed parallel and in a spaced relationship to the substrate 13. The object beam 17 penetrates the mask 45 and the transmitted light of the object beam interferes with the reference beam 19.

For forming a large-size hologram the reference and object light beams are preferably scanned in an aligned relationship across the entire mask 45 and substrate 13 surfaces in a raster scan-and-step operation whereby the object and the reference beams 17,19 interfere with each other in the holographic recording medium 15 thereby forming the desired hologram.

For the formation of holograms of a rather small size i.e. up to 2 square inches, no scanning of the beams is necessary.

The reconstruction of an image from the hologram requires that the direction of the reference light beam is reversed, i.e. being in the opposite direction to that of the reference beam in the hologram formation process. The interaction of the reversed light beam (=reconstruction beam) with the hologram produces a positive image of the circuit pattern in the photosensitive layer of e.g. a silicon wafer placed at the exactly same position as the mask in the hologram formation process (arrow .. indicates the reconstructed light beam).

In order that the image generated from the hologram is printed in focus in the photosensitive layer, the hologram bearing substrate and the wafer are made parallel and the separation between them is adjusted to the same distance as between the mask 45 and the recording layer 15 during the hologram formation process. For this purpose the wafer is mounted e.g. to a vacuum chuck which is positioned on adjustable supports, e.g. piezcelectric transducers. The local separation between the hologram and the photosensitive layer is interferometrically measured by a light beam. The light beam is scanned either beforehand or, preferably, simultaneously with the exposure beam scanning across the hologram surface. For each measurement point the interference

of the reflections from hologram and the wafer surface is detected from which the local separation between the hologram and the photosensitive layer is determined. As the light beam scans the hologram the distance between the hologram and the wafer, where the beam is illuminating the hologram, is continuously measured and then adjusted to the required value (corresponding to the distance between the recording layer and mask during hologram recording).

In order to account for the different cross-sections of the reference and object beams 17,19 a prism 49 is provided in the light path of the reference beam which compresses the reference beam in one direction.

According to the invention it is of importance that a photoresist is selected as the holographic recording medium, i.e. the interference of the object beam transmitted by the mask with the reference beam is recorded as a modulation of the layer thickness. Further, the planes of polarisation of the object and reference beams incident on the holographic recording medium are arranged such that their polarisation vectors are also substantially mutually orthogonal in the holographic recording medium and such that the polarisation vectors of the incident and totally internally reflected reference beams are substantially orthogonal. The latter can be achieved by providing polarisation means 51,53 in the light paths of the object and reference beams 17,19.

The total internal reflection holographic system according to the invention has polarisation means, e.g. polarisation rotation plates 51,53, which are arranged in the light path of the object and reference beams 17,19, respectively, for polarising the object and the reference beams so that not all possible holograms are formed (see figure 3).

It is to be noted that for the purpose of the present invention scanning of the reference and object beams is not an essential feature and that, accordingly, also stationary expanded beams can be used as disclosed in US 4,966,428 to Phillips.

Further details of the invention and experimental details are given hereinbelow.

I. Introduction

I.1. Technology trends and investment costs

Semiconductor chips have been miniaturised continuously since integrated circuit (IC) chips were introduced in 1965. The packing density of chips in mass production is now in the range of ~ 256 mega-bit dynamic random access memory (DRAM) with a minimum feature size of ~ 0.2 μm. The recent road map predicts that a 1 giga-bit DRAM with 0.18 μm and a 4 giga-bit DRAM with 0.15 μm features will appear on the market in 1999 and 2001, respectively[1]. The choice of lithography technology is of prime importance in meeting these targets. The technologies to manufacture these two generations of memory devices are tentatively optical lithography with KrF (λ=248nm) or ArF excimer lasers (λ=193nm) even though they barely satisfy technical specifications. However, these technologies might not be cost effective.

Among alternative feasible technologies, besides optical lithography, to fabricate such devices are: e-beam lithography, ion beam lithography, and X-ray lithography[2,3]. Each technology has its own restriction to chip production. Optical lithography with KrF excimer lasers requires complicated photomasks (phase-shift [4,-6] and masks corrected for optical-proximity-effect[7-9]) and processes (multi-layer resists[10-12], anti-reflection layers[13-15], top-surface imaging methods[16-18], etc.) to enhance image resolution and process latitude. Optical lithography with ArF excimer lasers suffers from unsolved problems such as compaction and color-center formation in optical components[19-21]. In addition, there is no suitable resist developed yet. Compared to other lithographic approaches, e-beam and ion beam lithographies are an order of magnitude slower because of writing directly onto a wafer[22]. Ion beam technology additionally leads to substrate damage and uses complicated stencil masks[23]. X-ray lithography needs a dedicated facility containing a synchrotron and magnetron as a light source, beam lines, X-ray steppers, etc. What is even more of a burden for X-ray lithography is the need for masks fabricated through a complex process. In addition, all exposure activity might be interrupted if the sole light source of synchrotron and magnetron stops for any reason. Even if optical lithography is feasible, it is no longer cost-effective. A step-and-scan optical lithographic system with a high numerical aperture (NA) of 0.63 equipped with a KrF excimer laser sourc or with an NA=0.6 and ArF illumination will cost approximately $7 million and $9 million/unit, respectively[24]. The semiconductor industry might hesitate to choose such a

tool in the future at these costs. The price of systems naturally increases because the number of lenses, their size, and the precision of their manufacturing has to increase. Moreover, the precision mechanics consisting of a wafer stage moving in the opposite direction to the mask stage at a 1:4 velocity ratio makes the machine extremely complex, hence expensive.

The imaging resolution, R, depends on the NA (NA= $\sin\theta$) of the optics used and is given by:

$$R = k_1 \frac{\lambda}{NA}, \qquad (I.1)$$

where k_1 is a process dependent constant and λ is the wavelength[25]. If the process constant is fixed, the resolution is proportional to λ and inversely proportional to NA. If the NA increases and/or λ decreases, the resolution is improved. If a technology with increased NA and without using sophisticated optics and mechanics emerges, people would choose it for future device manufacturing. For this reason, a new lithographic tool using total-internal-reflection (TIR) holography[26-32] might be one of the best candidates.

I.2. Why surface-relief TIR holography for deep ultra-violet (DUV) light?

F.S.M. Clube explained the principle of holographic lithography[33]. He claimed that the advantages of this technology are: (i) high effective NA (~0.8), (ii) readily scalable for large patterns (there is no compromise between resolution and field size), and (iii) no aberrations that degrade feature size uniformity and overlay.

TIR holography can be accomplished using either a volume or a surface-relief hologram. Volume TIR holography, using a refractive index modulation inside the hologram material, is subject to diffraction efficiency variations with a small change of thickness across the hologram plate or from plate to plate[34]. If the diffraction efficiency varies, the necessary exposure dose changes. To ensure a consistent efficiency, one needs to control the hologram thickness variation by strictly controlling temperature and humidity. Moreover, the thickness control may become more difficult if the wavelength decreases. Luckily, there are suitable materials in use

for volume holography for the ultra-violet (UV) regime whose wavelength ranges from 300nm to 400nm[35-38].

But if the wavelength goes down to a DUV, the deep ultra-violet, regime (λ~200-300nm) to achieve a high resolution, there is no suitable material for volume holography. Instead, surface-relief TIR holography can be considered as an alternative to the volume TIR holography. Because the effective refractive index modulation of the surface-relief hologram is higher than that of the volume by several orders of magnitude, the thickness can be reduced to <<1μm. The transmittance of numerous materials then remains in the reasonable range at say >50%. However, people worry about a peel-off problem of hologram layers during development, if a surface-relief technique is employed[39]. Such a peel-off problem may be overcome by a proper combination of polarisations for the reference and the object beams. Using a conventional etching technique such as plasma etching, it is possible to transfer the surface-relief image into its substrate to generate a stable hologram.

II.3. Evaluation of hologram materials

Since there are no DUV materials commercially available for volume holography, it is necessary to consider the alternative of surface-relief holography. Surface-relief holography uses the surface modulation with, while volume holography uses the index modulation between the exposed and unexposed fringes in the material. Since the index difference between air and the hologram material of surface-relief holography is in the range of 0.5-1.0, while that of the volume hologram is ~0.006, the hologram depth can be reduced by a factor of ~100. Therefore, even shallow surface modulation can give rise to the equivalent diffraction efficiency of the volume holography. This is advantageous because one can use a thin material (<1μm), which is standard in photolithography.

For DUV surface-relief holography, photoresists may be acceptable because they have long been used for photolithography. However, it is worthwhile to examine other materials such as dichromate poly-vinyl-alcohol (DC-PVA)[10-14] and poly-methyl-methacrylate (PMMA)[15,16], which have been studied extensively by other researchers using UV light. Another kind of resist worthy of study is silicon containing resist, GR650[17-22], which later can be converted to a glassy material after oxygen exposure. In this section, all candidate materials for the DUV surface-relief holography are compared from the point of view of resolution of the spatial frequency, sensitivity, linearity, etc. One cannot evaluate all possible

materials using the TIR holographic set-up, because it would require a lot of work. One selects therefore only a few suitable materials using the transmission set-up.

Refractive indices and extinction coefficients are measured using a spectroscopic ellipsometer. Results are summarised in Table II.1. The corresponding transmittance for 1µm thickness is shown.

Figure II.9. shows the intensity distributions inside the materials for the case of a) SAS001, b) SNR240, and c) DC-PVA at a thickness of 1µm. The light intensity decreases with the depth. The attenuation depends on the absorption coefficient α, determined from $\alpha=4\pi\kappa_{257}/\lambda_0$ with the extinction coefficient κ_{257} at $\lambda_0=0.257\mu m$. It is more difficult to obtain a good resolution with a highly absorbing material than a low absorbing one. If the intensity at the depth of 1µm drops by a factor <0.37, the risk to obtain features with bridgings between lines is strongly increased after processing. From this point of view, only seven materials such as SNR240, XP9549Q, DP009, PAR, SAS001, PMMA, and GR650 satisfy the low loss requirement for TIR holography.

Materials	Makers	Tone	n_{257}	κ_{257}	T/µm	Sensitivity (mJ/cm²)	γ	Resolution
SNR240	Shipley	Nega.	1.8	0.01	0.61	30	1.2	65 nm
XP7157	Shipley	Posi.	1.81	0.03	0.23	30	11.2	85 nm
XP9549Q	Shipley	Posi.	1.67	0.011	0.58	32	2.1	80 nm
UV-XII	Shipley	Posi.	1.71	0.035	0.18	32	6.8	80 nm
SPR505	Shipley	Posi.	1.961	0.135	0	105	3.3	110nm
DP009	TOK	Posi.	1.738	0.016	0.46	70	6.5	70 nm
N908	TOK	Nega.	1.82	0.04	0.14	188	8.6	70 nm
IP3300	TOK	Posi	1.823	0.196	0	120	5.8	80nm
PAR	Sumitomo	Posi.	1.789	0.007	0.71	265	31	100 nm
SAS001	Samsung	Posi.	1.66	0.005	0.78	266	32	60 nm
SAS002	Samsung	Posi.	1.77	0.029	0.24	250	1.89	100 nm
PFI58A7	Fuji	Posi.	1.791	0.134	0	110	3.6	120nm
DC-PVA	Aldrich	Posi.	1.48	0.033	0.33	188	1.93	150 nm
PMMA	All resist	Posi.	1.77	0.011	0.58	1500	1.58	60 nm
GR650	Technegias	Nega.	1.62	0.019	0.39	55	1.3	700 nm

n_{257}: refractive index at λ_0=257nm κ_{257}: extinction coefficient at λ_0=257nm
T=exp(-αt) for t=1μm

Table II.1. Optical properties of the potential materials for DUV surface-relief holography. All values are valid for λ=257nm.

But if the thickness becomes as thin as 250nm, which is still thick enough for plasma etching applications, the transmittance at this depth would increase significantly. The materials: SPR505, IP3300, and PFI58A7 practically have zero transmittance at 1μm thickness. The transmittance for 250nm thickness is only 0.19, 0.09, and 0.19, respectively. All these values are still smaller than 0.37. These materials have high absorption as they contain highly UV absorbing aromatic groups as back-bones[23-25]. These three materials are eliminated.

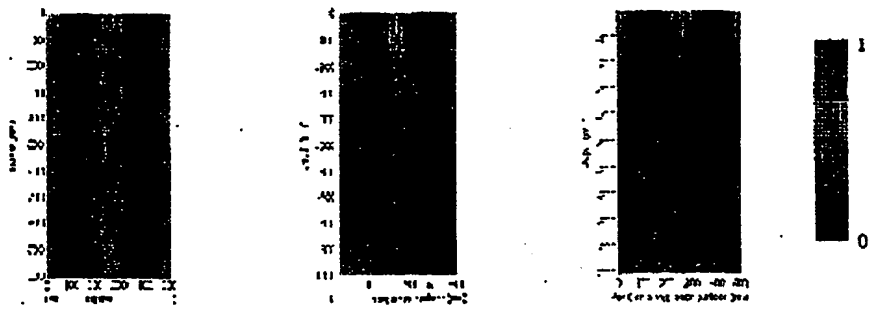

Fig. II.9. Relative intensity distributions with S-polarisation in three different materials having different transmittances: a) 0.78/μm, b) 0.61/μm, and c) 0.32/μm.

Materials which pass the absorption screening undergo the exposure test to find the photosensitivity, the γ-value, and the resolution. The photosensitivity is inferred from the γ-

curve with $((E_1+E_0)/2)$. The angle of incidence is varied to change the minimum period. Table II.1. summarises the results from extensive experimental studies.

The photosensitivity of PMMA is far inferior to that of other materials. It will take a fairly long exposure time to expose the full thickness of this material. In this case, stable hologram formation must be very difficult because any disturbance induced during long exposure such as floor vibration, acoustic vibration, air turbulence, etc. becomes important. Therefore, all materials having poor sensitivities (<100 mJ/cm^2) are also rejected.

Because the γ-value is related to the slope of the γ-curve, low γ-values tend to transfer images more faithfully. Therefore, all the materials having reasonably low contrast such as γ<3 are chosen. Among the six chosen resists, SNR240 shows the lowest γ-value with γ=1.2.

For the resolution capability test, the modulation depth is measured for different grating periods. The modulation contrast, M, is given: $M=(d_{max}-d_{min})/(d_{max}+d_{min})$, where d_{max} and d_{min} are the thicknesses of the resist corresponding to the crest and the trough of the grating. These M-values are not shown in Table II.1. Resist features with M-values lower than 0.25, corresponding to $d_{max}=1$ and $d_{min}=0.6$, are considered to be unresolved hence rejected. The resolution capability is the best for SNR240 with a feature size of 65nm, while DC-PVA and GR650 show poor resolution. Both XP9549Q and SAS002 have a resolution capability inferior to SNR240, although most of the properties of XP9549 Q are quite similar to those of SNR240. Its resolution capability of 80nm is satisfactory for DUV TIR holography. But it is worthwhile to demonstrate the effect of such a small γ-value difference. Figure II.10. shows the exposure signals with a) four different exposure doses, and their corresponding calculated resist-profiles for b) SNR240 with γ=1.2 and c) XP9549Q with γ=2.1. It is difficult to notice any difference concerning the linearity between the two profiles except for the reversed tone (one negative and the other positive). This means that either of these two resists are satisfactory. For our experiments on the TIR set-up, negative tone is preferable. With the TIR set-up, because the strong reference beam with respect to the object beam irradiates the hologram layer from the bottom, a strong intensity may be distributed near the bottom of the hologram layer. In this case, if the hologram material is a positive tone, the developer liquid will quickly dissolve the strong intensity area along the interface between the hologram layer and the substrate. This may cause a pattern-lifting problem.

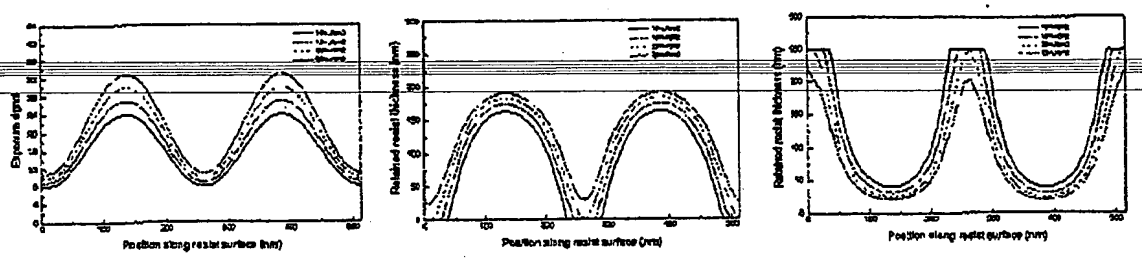

a) b) c)

Fig. II.10. Exposure doses and their corresponding calculated resist profiles.
a) Exposure doses, b) calculated resist profiles for SNR240, and c) those for XP9549Q.

As far as the resolution capability in this screening procedure is concerned, a steep profile is not essential, unlike to conventional lithography. Sinusoidal profiles can be achieved with low γ-values. But DC-PVA whose γ-value is low (γ=1.95) does not show this phenomenon. Sinusoidal profile with DC-PVA was observed down to 500nm. But features below this size lose recording fidelity as shown in Fig. II.11.a). The profile is no longer sinusoidal. Feature sizes below 350nm are not resolved. Only a plane material surface is observed. This is presumably due to swelling during processing because PVA is water soluble. It is vulnerable to moisture[10], and therefore wet processing using water is potentially risky. Figure II.11.b) shows SNR240's 65nm resolution capability with good fidelity to a sinusoidal intensity profile. Therefore, any interference fringe made from DUV TIR holography near this size can be resolved as such.

For most parts of this thesis, experimental and simulation results are for SNR240. Further characterisation of this resist will be shown in the following chapters.

a) b)

Fig. II.11. Cross-sectional profiles of the patterns in a) DC-PVA and b) SNR240. The smallest features obtained with each material are 350nm and 65nm, respectively.

III. TIR holography

One of the major advantages of TIR holography is that it is possible to record a large image field with a high NA because of the proximity between the object and the hologram[1-3]. However, TIR holography indispensably needs a third beam, the TIR beam, along with the object and the reference beams that cause a complicated intensity distribution within the hologram layer. Since surface-relief holography uses the strong index difference between the air and the hologram grating, a deep surface modulation in general will deliver a high diffraction efficiency. Because the intensity distribution is a function of many factors such as the angle of incidence, polarisations of the object and the reference beams, beam intensity ratio, absorption and refractive index of the hologram material, etc., the effect from each factor should be examined to achieve the best surface modulation.

The aim of our work for TIR holography is to maximise resolution with good diffraction efficiency. For surface-relief, aims are to achieve sufficient modulation depth with a linear recording and zero noise. These depend on intensity distribution and process parameters, all of which require optimisation.

In this chapter, a brief theory, extended simulation along with experimental results are shown. A way to achieve a good surface modulation is also presented by changing process parameters. The modulation depth is measured by a scanning electron microscope (SEM) or an atomic force microscope (AFM).

III.1. Theory

In TIR holography, three beams contribute to the formation of interference fringes inside the hologram material. Figure III.1. illustrates the three beams incident on the recording material of photoresist. The prism used for the calculation and the experiment is an isosceles triangle with an apex angle of 90°. The electric fields, $\mathbf{E}_r$, $\mathbf{E}_{rr}$ and $\mathbf{E}_o$, for these three beams can be expressed as

$$\mathbf{E}_r = E_r \cdot \mathbf{P}_r \cdot \exp(i \cdot \mathbf{k}_r \cdot \mathbf{r}), \tag{III.1}$$

$$\mathbf{E}_{rr} = E_{rr} \cdot \mathbf{P}_{rr} \cdot \exp(i \cdot \mathbf{k}_{rr} \cdot \mathbf{r}), \text{ and} \tag{III.2}$$

$$\mathbf{E}_o = E_o \cdot \mathbf{P}_o \cdot \exp(i \cdot \mathbf{k}_o \cdot \mathbf{r}), \qquad \text{(III.3)}$$

where E_{ir}, E_{rr}, and E_o are the electric field amplitudes; $\mathbf{k}_{ir}$, $\mathbf{k}_{rr}$, and $\mathbf{k}_o$ are the complex wave vectors of the electric fields of the incoming reference, reflecting reference, and object beams respectively, with $\mathbf{r} = x\hat{x} + y\hat{y} + z\hat{z}$; $\mathbf{k}_{ir} = \frac{2\pi}{\lambda_0}(n_{pr} + i\kappa)(-\sin\theta_{pr}, 0, -\cos\theta_{pr})$, $\mathbf{k}_{rr} = \frac{2\pi}{\lambda_0}(n_{pr} + i\kappa)(-\sin\theta_{pr}, 0, \cos\theta_{pr})$, and $\mathbf{k}_o = \frac{2\pi}{\lambda_0}(n_{pr} + i\kappa)(0,0,1)$; θ_{pr} is the incident angle of the reference beam within the hologram material; n_{pr} and κ are the refractive index and the extinction coefficient, respectively. $\mathbf{P}_{ir}$, $\mathbf{P}_{rr}$, and $\mathbf{P}_o$ are the polarisation vectors. If a linear polarisation is considered, each polarisation vector is expressed as:

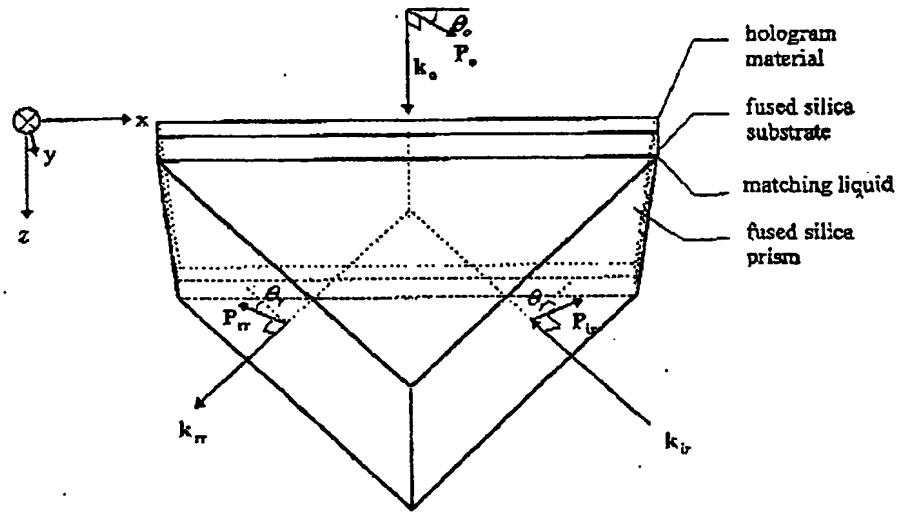

Fig. III.1. Geometry of TIR holography.
(x,y): layer plane.

$$\mathbf{P}_{ir} = \begin{pmatrix} \cos\theta_r \cos\theta_{pr} \\ \sin\theta_r \\ -\cos\theta_r \sin\theta_{pr} \end{pmatrix}, \tag{III.4}$$

$$\mathbf{P}_{rr} = \begin{pmatrix} -\cos\theta_r \cos\theta_{pr} \cos p \\ \sin\theta_r \cos s \\ -\cos\theta_r \sin\theta_{pr} \cos p \end{pmatrix} + i \begin{pmatrix} -\cos\theta_r \cos\theta_{pr} \sin p \\ \sin\theta_r \sin s \\ -\cos\theta_r \sin\theta_{pr} \sin p \end{pmatrix}, \text{ and} \tag{III.5}$$

$$\mathbf{P}_o = \begin{pmatrix} \cos\theta_o \\ \sin\theta_o \\ 0 \end{pmatrix}, \tag{III.6}$$

where θ_r and θ_o are the azimuthal angles of polarisation off the plane of incidence for the reference and the object beams, respectively; p and s are the phases shifted due to the total internal reflection for polarisation components of P- and S-polarisations, respectively and are expressed as

$$p = 2\cdot\tan^{-1}\left(-\sqrt{\sin^2\theta_{pr} - 1/n_{pr}^2}\,/\,(1/n_{pr}^2\cdot\cos\theta_{pr})\right) \text{ and} \tag{III.7}$$

$$s = 2\cdot\tan^{-1}\left(-\sqrt{\sin^2\theta_{pr} - 1/n_{pr}^2}\,/\cos\theta_{pr}\right), \tag{III.8}$$

where n_{pr} is the refractive index of the photoresist. The average electric field energy density, I, within the hologram material can be expressed as:

$$I \propto \left(\mathbf{E}_{ir} + \mathbf{E}_{rr} + \mathbf{E}_o\right)\left(\mathbf{E}_{ir} + \mathbf{E}_{rr} + \mathbf{E}_o\right)^*. \tag{III.9}$$

Figure III.2.a) illustrates the decomposition of the three beams into three groups of two mutual beams interfering each other to produce corresponding fringe sets. Fringes are formed by the incoming reference and the object beams; by the TIR and the object beams; by the incoming and the TIR beams are referred to as reflection, transmission and Lippmann holograms respectively[4].

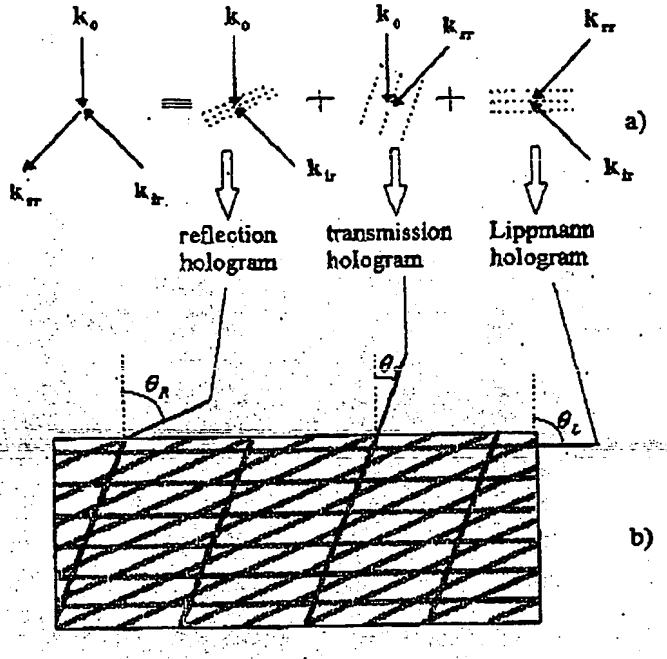

Fig. III.2. Illustration of fringe formation within the hologram material by TIR holography: a) Three different hologram fringes formed by two mutually coherent beams. b) Three holograms superposed on top of each other within TIR hologram.

These three holograms are formed in a hologram layer with different inclination angles denoted as θ_R, θ_T, and θ_L for the reflection, the transmission, and the Lippmann holograms, respectively as shown in Fig. III.2.b). The three inclination angles θ_R, θ_T, and θ_L will be ~ 72°, – 18°, and 90° respectively, if the refractive index of the hologram material is taken as 1.8. The grating periods for the reflection, the transmission, and the Lippmann holograms are 75nm, 231nm, and 88nm, respectively.

Since the intensity distribution within the hologram material is a function of many different parameters such as absorption, thickness, refractive index of the material, polarisation, incident angle, and beam intensity ratio between reference and object beams, the shape of interference fringe might vary with different combinations of such parameters. From eq. (III.1) to (III.3), it is possible to group the parameters: one set of parameters is related to the properties of the resist and the other set depends on the optics. The following sections deal with these sets.

III.1.1. Effect of resist parameters

Since three beams interfere with each other, the influence of the resist parameters such as absorption, refractive index, and resist thickness are considerably more complicated than with two beam interference. To obtain a deep surface modulation after recording and processing, it is worthwhile to show the effect of these parameters.

III.1.1.1. Absorption effect

The absorption effect in the TIR hologram is closely related to the intensity contrast differences among the three different hologram fringes. However, it is not so simple to conjecture the distribution because all three fringes yield a lot of nodes and anti-nodes. Figure III.3. shows the intensity distributions within the hologram material for various absorption coefficients corresponding to 0/μm, 0.48/μm, and 1.42/μm with P-polarisation for both the object and the reference beams. Those three absorption coefficients correspond to lossless material, Shipley resists SNR240 or XP9549Q, and Samsung resist SAS002, respectively.

Intensity distributions are shown in Fig. III.3. using P-polarisation for both the reference and the object beams with 1:1 beam intensity ratio between the two beams. In Fig. III.3.a), the transmission and the reflection holograms are clearly visible, while there is no distinct Lippmann hologram. However, with increasing absorption, the transmission grating gradually disappears going through the depth of the resist. For SAS002, even the reflection hologram shows only a weak contrast, which can be interpreted as both the object and the reference lights being strongly absorbed while they travel through the resist. For any of the three cases, the crossing of the transmission hologram with the reflection hologram creates new nodes and anti-nodes. This makes it difficult to go through the depth from the surface of resist during development. The first node group from the surface might be peeled off, if the resist is over-developed. Therefore, the development condition should be precisely controlled.

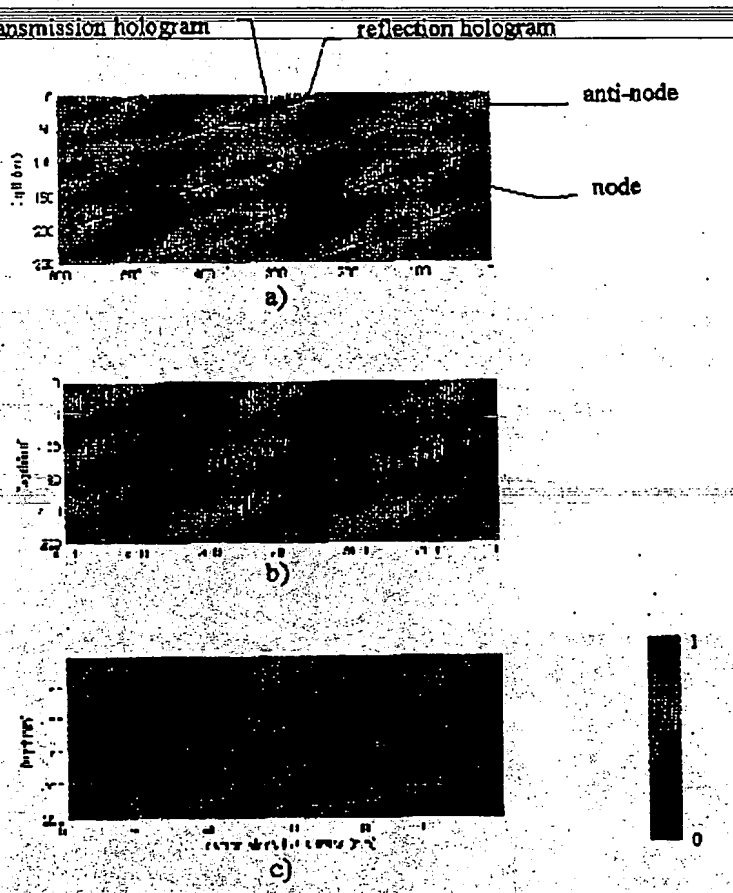

Fig. III.3. Intensity distributions within hologram layers with different absorption coefficients: a) 0/μm, b) 0.48/μm, and c)1.42/μm, which correspond to a lossless material, SNR240/XP9549Q, and SAS002, respectively. P-polarisation is used both for the object and the reference beams.

As the absorption increases, the reflection hologram becomes dominant because the weakened TIR beam with the object beam makes a weak transmission hologram. In this case, the developer solution will more rapidly penetrate along the reflection hologram, which might cause collapsed patterns due to significant inclination of the fringes.

If the slightly absorbing resist, SAS002, is carefully developed, it is possible to obtain a surface modulation without causing pattern collapse. But the development latitude before the pattern collapses

is very small. While the development proceeds, the general surface will also be eroded, resulting in rounded profiles.

Figure III.4. shows two cross-sectional profiles after development of SNR240 and SAS002. SAS002 was developed for only 5s in a developer, Shipley MF322, to avoid the pattern collapse, while SNR240 was dipped in the same developer for 30s. The degree of the surface modulation of SNR240 is distinctly higher than that of SAS002. The degree of pattern inclination is also very high as is predicted from the simulation. In practice with SAS002, it is almost impossible to avoid pattern collapse, if the development time increases to improve the surface modulation depth. This underlines the fact that low absorption materials such as SNR240 and XP9549Q are more suitable for the surface relief TIR holography.

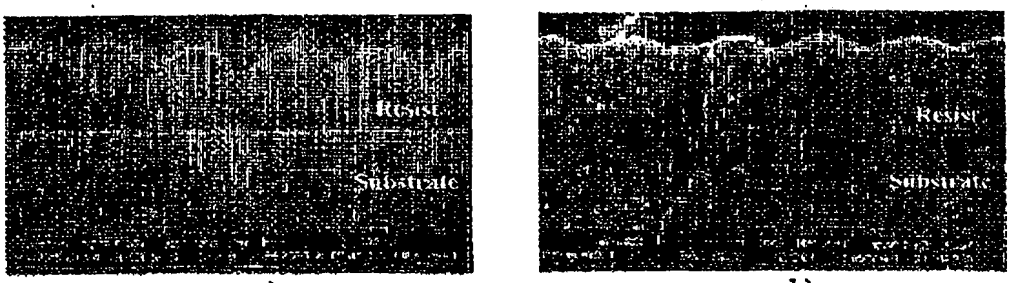

a) b)

Fig. III.4. Cross-sectional profiles of a) SNR240 and b) SAS002 recorded with DUV TIR holography.

III.1.1.2. Refractive index effect

For the intensity distribution, the index of refraction is another important parameter of the resist. The refractive index in surface-relief holography is important not only for taking into account of the reflection but also for the diffraction efficiency which is directly coupled to the index difference between the resist and the air. Figure III.5. shows the intensity distribution within the resist with three different refractive indices of 1.5, 1.67, and 1.8 at λ_0= 257nm. These three refractive indices correspond to materials whose indices are close to the fused silica substrate, for XP9549Q, and for SNR240, respectively.

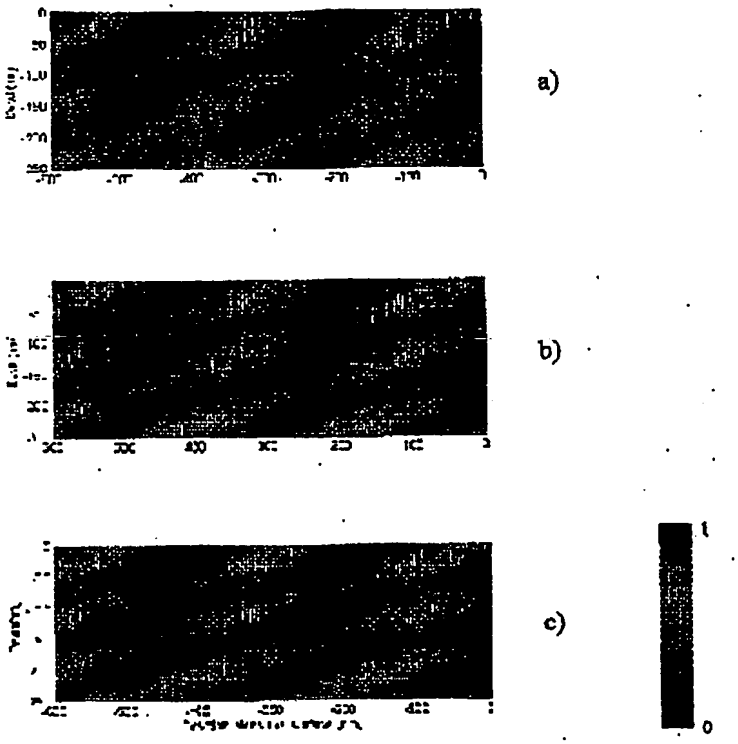

Fig. III.5. Intensity distributions within hologram layers with different refractive indices: a) 1.5, b) 1.67, and c) 1.8, which correspond to a material having a similar index to the fused silica substrate, XP9549Q, and SNR240, respectively.

As the index increases, the grating period of the reflection hologram is shortened, while that of the transmission stays essentially unchanged. This can be explained with the Ewald circle diagrams shown in Fig. III.6. The radius in the diagram represents the magnitude of the wavevector, $k = 2\pi n / \lambda_0$. As the refractive index, n, increases, the radius of the circle increases and both the incident and the TIR angles, θ_{2i} and θ_{2r} become smaller than θ_{1i} and θ_{1r}. Therefore, the resulting grating vector for the reflection hologram, $|\mathbf{K}_{2r}|$, becomes larger than $|\mathbf{K}_{1r}|$. This means that the grating period with a higher refractive index becomes shorter than that with a lower refractive index. For the transmission hologram, $|\mathbf{K}_{2t}|$ becomes only slightly smaller than $|\mathbf{K}_{1t}|$. This shallow depth modulation with a higher refractive index

will be a disadvantage in view of signal to noise (S/N) ratio. Even though the modulation depth is shallow, the diffraction efficiency will not be very different due to the enhanced index difference between the resist and the air. However, for a rough resist surface, the noise level caused by a fixed degree of roughness is expected to be higher for a large index than that for a small index. Therefore, materials with lower index are more suitable.

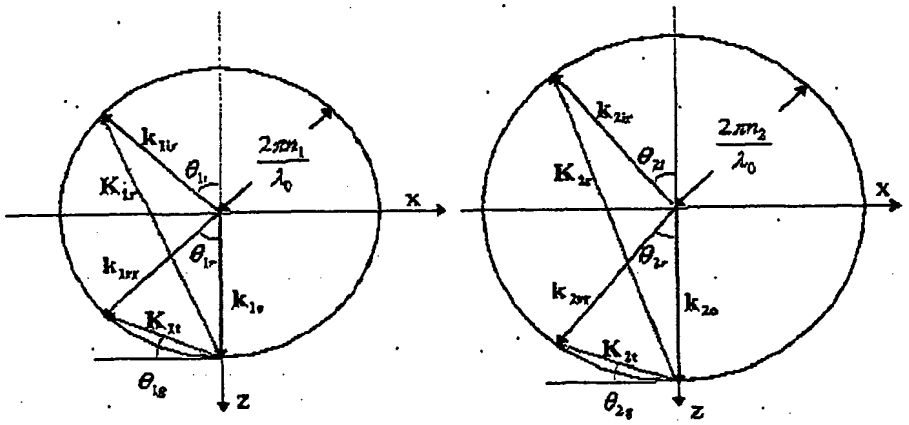

a) b)

Fig. III.6. Circle diagrams for a) low and b) high refractive indices, showing the wavevectors of the three recording waves and the corresponding grating vectors. For $n_2 > n_1$, the magnitudes of the grating vectors of $|\mathbf{K}_{2t}| = |\mathbf{K}_{1t}|$, while $|\mathbf{K}_{2r}| > |\mathbf{K}_{1r}|$.

III.1.1.3. Thickness effect

Since the resist thickness (d) is coupled with the absorption coefficient (α) to determine the transmittance (T) of the resist through a formula $T = \exp(-4\pi\kappa/\lambda_0)\cdot d = \exp(-\alpha\cdot d)$, the product $\alpha\cdot d$ is of prime concern. As mentioned earlier, the thickness should be reduced to satisfy $\alpha\cdot d < 1$ to have low absorption. Fortunately, the thickness of the resist can be easily adjusted by diluting the liquid resist with solvent and/or by changing the speed of a spin-chuck, while the absorption is fixed only by the solidified resist. However, the density of defects such as pinholes, voids within the resist, and dimples on

the resist surface, dramatically increases with decreasing thickness of the resist[5]. If there are such defects within the resist, patterns will peel off during development or rinsing. Figure III.7.a) shows the defects revealed after development of the 75nm thick resist, SNR240, while b) shows no defects with a 300nm thick resist. The thinnest resist thicknesses free from the defects are 200nm, 220nm, and 180nm for SNR240, XP9549Q, and SAS002, respectively. The development time for this defect test was 30s with 1:1 diluted MF322 developer. Even if the void within the resist layer is not exposed during development, it may be revealed during the dry etching that erodes the resist along with the substrate.

The task of reducing defects is more one of prevention than of actual elimination, since the reliable accuracy of rapid testing is limited to about 0.25µm, the detection limit of an optical microscope. Nevertheless, there are some observations and procedures which should minimise their occurrence: clean surface, ultrafiltration of resist to remove gels and insolubles, highest prebake temperature to flow resist, etc. Therefore, the resist thickness should be determined taking into account of the resist's defect density, and etching process conditions. To be on the safe side, we choose 250nm, 270nm, and 230nm thicknesses for SNR240, XP9549Q, and SAS002, respectively for our later experiment.

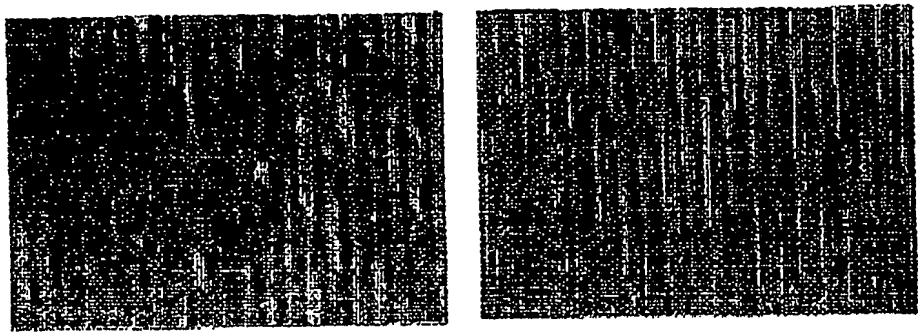

a) b)

Fig. III.7. Gratings (period of 257nm) formed with different resist thicknesses:

a) Defects with 75nm thick resist. b) No defects with 300nm thick resist.

III.1.1.4. Summary

In summary, it is desirable to find a resist material which has high transparency and low refractive index with a defect-immune thickness. Two resists of SNR240 and XP9549Q have equally low absorption α=0.48/μm. But SNR240 has higher refractive index (1.8) than XP9549Q (1.67). In view of defect free thickness for these two resists, SNR240 (250nm) is slightly better than XP9549Q (270nm). These two resists will be compared from scattering point of view in chapter IV.

III.1.2. Effect of optical parameters

III.1.2.1. Effect of polarisation

If all the three holograms resulting from the three beam interference are equally strong in intensity, the intensity distribution will be very complicated as indicated in Fig. III.2. For this case, the surface modulation depth after processing will be very shallow as we have already demonstrated with only two holograms (the transmission and the reflection holograms). One of the optical parameters affecting the intensity distribution within a resist is the polarisation, as predicted from eq. (III.1) to (III.3). Since polarisation changes the relative strengths of the three holograms within the resist, it would be useful to find the best combination of the polarisation for the object and the reference beams.

III.1.2.1.1. TIR holography without photomask

It is easy to imagine how the intensity distribution looks, if only two beams are interfering with each other for different polarisation angles. But when three beams are involved with different polarisation vectors, it becomes quite difficult to visualise the intensity distribution. The Lippmann hologram can nearly be eliminated by employing P-polarisation for both the incoming reference and the object beams. But in this case, the other two holograms, the transmission and the reflection holograms, still exist in the resist which superpose as shown in Fig. III.3. This might be a problem in obtaining a deep surface modulation after development. It would be useful, if a certain polarisation combination of the reference and the object beams eliminates the reflection hologram, the residual Lippmann hologram that crosses the transmission hologram would have a longer period (88nm).

From the condition $\mathbf{P}_{ir} \cdot \mathbf{P}_{o} = 0$ in eq. (III.4) and (III.6) to eliminate the reflection hologram, one gets

$$\tan\theta_r \cdot \tan\theta_o = -\cos\theta_{ir}. \qquad \text{(III.10)}$$

And the maximum and the minimum intensities for the Lippmann and the transmission holograms are

$$I^{L}_{max,min} = \mathbf{E}^2_{ir} + \mathbf{E}^2_{rr} \pm 2\mathbf{E}_{ir}\mathbf{E}_{rr}\left|\mathbf{P}_{ir} \cdot \mathbf{P}_{rr}\right| \text{ and} \qquad \text{(III.11)}$$

$$I^{T}_{max,min} = \mathbf{E}^2_{rr} + \mathbf{E}^2_{o} \pm 2\mathbf{E}_{rr}\mathbf{E}_{o}\left|\mathbf{P}_{rr} \cdot \mathbf{P}_{o}\right|, \qquad \text{(III.12)}$$

respectively. If $\mathbf{E}_{rr} = \mathbf{E}_{ir}$ (for loss-less material) and the amplitude ratio, $r = \mathbf{E}_{o} / \mathbf{E}_{ir}$, the intensity contrast, for each hologram becomes as follows:

$$C_{Lipp} = \left|\mathbf{P}_{ir} \cdot \mathbf{P}_{rr}\right| \qquad \text{(III.13)}$$

for the Lippmann hologram and

$$C_{trans} = \frac{2r}{1+r^2}\left|\mathbf{P}_{rr} \cdot \mathbf{P}_{o}\right| \qquad \text{(III.14)}$$

for the transmission hologram.

Figure III.8. shows the contrast for each hologram as a function of the polarisation angle for the reference beam in the case of the amplitude ratio r=1. The contrast of the transmission hologram is always higher than that of the Lippmann hologram with the polarisation angle between 8° and 59°, while keeping that of the reflection hologram to zero. There is one particular angle, θ_r, which generates a high contrast of the transmission hologram with a very low contrast of the Lippmann hologram. This angle is θ_r=29° with its corresponding angle for the object beam, θ_o=-56° according to eq.(III.10). If the intensity contrast is too low, e.g. C<0.4, the surface modulation might not be deep enough. In this case, the top surface might be quickly eroded during development. This shallow surface modulation was experimentally confirmed using SNR240 resist with the transmission set-up with an inter-angle of 70° having P-polarisation, which corresponds to C=0.4. In this case, the useful range of polarisation angle is limited between 12° and 44°. If the absorption is taken into account, the

contrasts for the Lippmann and the transmission holograms might be slightly decreased because $E_{rr} \neq E_{tr}$.

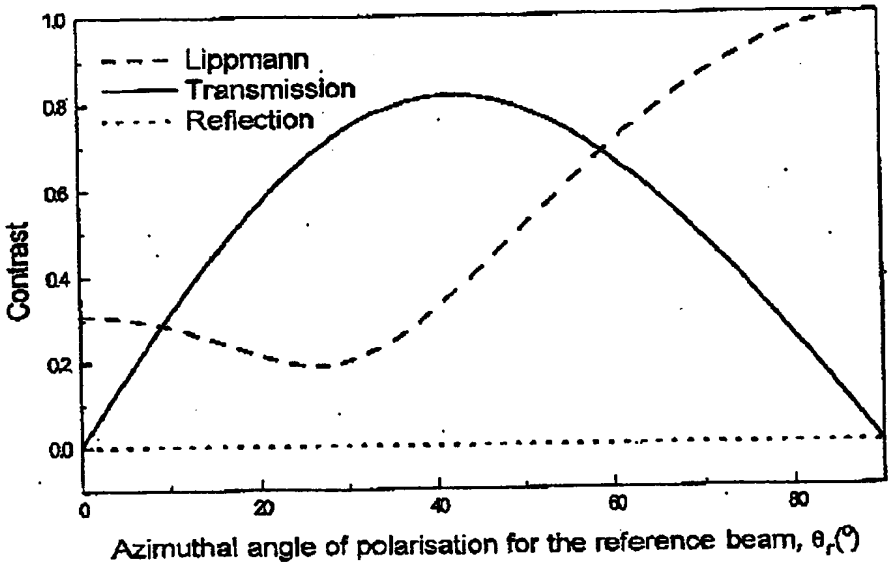

Fig. III.8. Contrast as a function of polarisation angles for the reference beam. The reflection hologram is eliminated.

Figure III.9. shows the intensity distributions for SNR240 resist with three different combinations of polarisation angles of the reference and the object beams. Eq. (III.10) is satisfied to get rid of th reflection hologram. The contrast of the transmission hologram for the reference polarisations of 39° and its corresponding object polarisation of -45° is the highest. Figure III.9.c) may generate weak modulation, because the contrasts for both the transmission and the Lippmann are weak. Figure III.8.b) shows a good transmission hologram with a weak Lippmann hologram. Therefore, it is suggested that the combination of polarisation angles for the reference and the object beams shall be chosen on the basis of the contrasts of the two different holograms.

Figure III.10. shows the resist profile developed with MF322 for 30s after recording with the polarisation combination of θ_r=29° and θ_o=-56°. Neither the reflection nor the Lippmann hologram is visible. This may come from the acid diffusion during post-exposure bake (PEB). The acid generated during exposure can be diffused during baking. The acids may diffuse along the transmission fringe than the Lippmann hologram at the PEB temperature of 110°C. The modulation depth in SEM

micrograph is ~200nm, which is deeper by a factor of ~4 than the depth made with P-polarised beams which was already shown in Fig. III.4.a). The modulation depths for Fig. III.9.a) and c) are 70nm and 40nm, respectively. The strong Lippmann hologram which blocks the development in the vertical direction for Fig. III.9.a) and the poor contrasts for Fig. III.9.c) are of the origin of the poor result in this case.

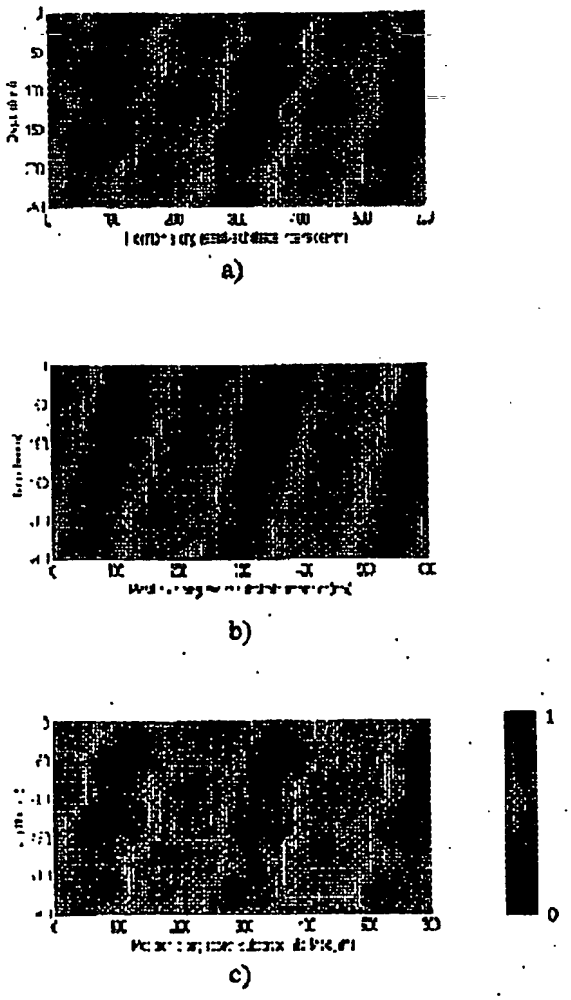

Fig. III.9. Intensity distributions for three different combinations of polarisation angles: a) θ_r=39° and θ_o= -45°, b) θ_r=29° and θ_o= -56°, and c) θ_r=19° and θ_o= -67°.

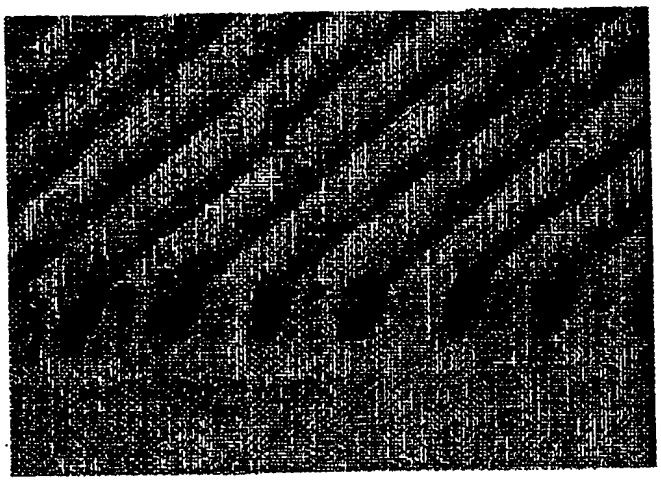

Fig. III.10. Developed resist profile recorded by the TIR holography with the polarisation angles of 29° and -56° for the reference and for the object beams, respectively. Neither the reflection nor the Lippmann holograms are observable.

III.1.2.1.2. TIR holography with photomask

We have considered TIR holography without using a photomask. In this case, only three major beams contribute to forming interference fringes with the hologram layer. For a photomask containing structures that are mutually orthogonal, the number of beams interfering each other will increase dramatically. This will generate numerous fringes. It may be possible to find the correct parameters to obtain strong fringes with the interference between the TIR and the diffracting beams from a photomask. The reflection and the Lippmann holograms should also be suppressed. Figure III.11.a) schematically represents the 3-dimensional geometry of the masked TIR holography showing $\pm 1^{st}$ orders for both in x- and y- directions. Figure III.11.b) shows how the diffracted beams travel across the hologram layer with their proper polarisation and refraction angles. To simplify the representation, the diffraction orders are considered only in x-direction. The notations used for calculations are as follows:

$\mathbf{k}_o^{0,0}$: 0th order object beam wave vector

$\mathbf{k}_o^{+\delta,0}$: +1st order object beam wave vector diffracted from the mask grating along x-axis

$\mathbf{k}_o^{-\delta,0}$: -1st order object beam wave vector diffracted from the mask grating along x-axis

$\mathbf{k}_o^{0,+\delta}$: +1st order object beam wave vector diffracted from the mask grating along y-axis

$\mathbf{k}_o^{0,-\delta}$: -1st order object beam wave vector diffracted from the mask grating along y-axis

$\mathbf{P}_o^{0,0}$: 0th order object beam polarisation

$\mathbf{P}_o^{+\delta,0}$: polarisation vector of +1st order object beam diffracted from the mask grating along x-axis

$\mathbf{P}_o^{-\delta,0}$: polarisation vector of -1st order object beam diffracted from the mask grating along x-axis

$\mathbf{P}_o^{0,+\delta}$: polarisation vector of +1st order object beam diffracted from the mask grating along y-axis

$\mathbf{P}_o^{0,-\delta}$: polarisation vector of -1st order object beam diffracted from the mask grating along y-axis

$\mathbf{P}_{ir}$: polarisation vector of incoming reference beam, not shown in Fig. III.11.

$\mathbf{P}_{rr}$: polarisation vector of TIR beam, not shown in Fig. III.11.

$\pm\delta'$: ± 1st order diffraction angle in air

$\pm\delta$: ± 1st order diffraction angle in hologram layer

θ_o : polarisation angle from x-axis around z-axis.

θ_r : polarisation angle for the reference beam

The diffracted polarisation vectors inside the hologram layer are expressed as follows:

$$\mathbf{P}_o^{0,0} = (\cos\theta_o, \sin\theta_o, 0) \qquad \text{(III.15)}$$

$$\mathbf{P}_o^{\pm\delta,0} = (\cos\theta_o \cos\delta, \sin\theta_o, \mp\cos\theta_o \sin\delta) \qquad \text{(III.16)}$$

$$\mathbf{P}_o^{0,\pm\delta} = (\cos\theta_o, \sin\theta_o \cos\delta, \mp\sin\theta_o \sin\delta) \qquad \text{(III.17)}$$

$$\mathbf{P}_{ir} = (\cos\theta_r \cos\theta_{pr}, \sin\theta_r, -\cos\theta_r \sin\theta_{pr}) \qquad \text{(III.18)}$$

$$\mathbf{P}_{rr} = (-\cos\theta_r \cos\theta_{pr} \cos p, \sin\theta_r \cos s, -\cos\theta_r \sin\theta_{pr} \cos p) + i(-\cos\theta_r \cos\theta_{pr} \sin p, \sin\theta_r \sin s, -\cos\theta_r \sin\theta_{pr} \sin p) \qquad \text{(III.19)}$$

For a desired minimum feature size of 0.15μm (corresponding to a pitch of 0.3μm), the 1st order diffraction angle δ' becomes 58.9° with an illumination wavelength of 257nm. Therefore, its refracted angle δ into the hologram material, SNR240 resist, becomes 28.4°.

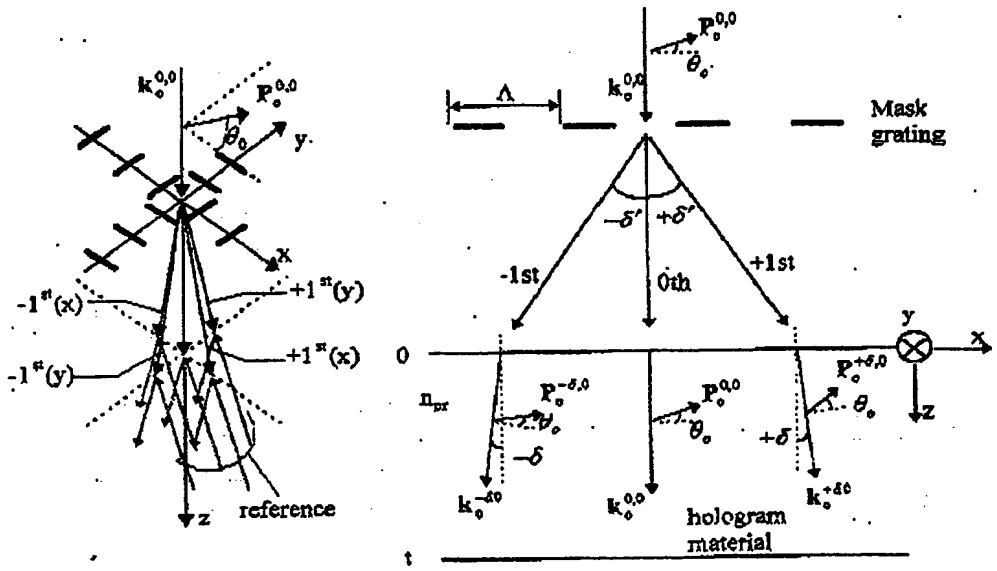

Fig. III.11. Geometry of the TIR holography with a periodic mask: a) Reference beams and +/-1st order diffracted beams from both x- and y-direction features on the mask. b) Notations of the diffraction orders in x-direction.

The fringe contrasts for the Lippmann and the transmission holograms in the hologram layer are given by eq. (III.13) and (III.14), respectively. The fringe contrast for the reflection hologram is given as follows:

$$C_{ref} = \frac{2r}{1+r^2}\left|\mathbf{P}_{ir}\cdot\mathbf{P}_{o}\right|, \qquad \text{(III.20)}$$

where r is the amplitude ratio between the object and the reference beams.

If the polarisation angle for the object beam were chosen such that the direction of $\mathbf{P}_o$ becomes common to both x- and y-direction features, features in both orientations would be produced with equal quality. This is achieved with the object polarisation angle, $\theta_o = \pm 45°$.

Because we want to suppress the fundamental reflection hologram formed by the interference between the 0^{th} order object beam and the reference beam, the fringe contrast should be kept to zero, that is $\left|\mathbf{P}_o^{0,0}\cdot\mathbf{P}_{ir}\right| = 0$. Even with this condition, the contrasts of the other reflection holograms formed with $\pm 1^{st}$ order diffracted beams cannot be completely cancelled. It is worthwhile to examine if they remain at minimum level.

Figure III.12. shows the contrast distribution calculated for the case of an assumed diffraction angle of 60° as a function of the reference and the object polarisation angles of θ_r and θ_o, respectively. The contrast map is drawn for different fringes formed with $\pm 1^{st}$ diffraction orders for the vertical and the horizontal gratings on the mask. The high contrast areas are distributed in diagonal directions. The high contrast stripes are running from the bottom-left to the top-right of corners for the interference group a) and from the bottom-right to the top-left of corners for b). These two groups look like mirror images of each other except for the cases of $\left|\mathbf{P}_{ir}\cdot\mathbf{P}_o^{\pm\delta,0}\right|$ and $\left|\mathbf{P}_{rr}\cdot\mathbf{P}_o^{\pm\delta,0}\right|$. The windows of the reference polarisation angles with the given object polarisation angle of -45° are shown in each contrast map. Low contrasts are chosen as the windows for a) and high ones are chosen for b). The common area for both a) and b) is 32° to 62° for the reference polarisation with -45° for the object polarisation. If -45° is chosen for θ_o, according to eq. (III.10), the θ_r becomes 39° that is within the common area.

If the contrast for a diffraction angle of 60° is acceptable, the contrast for diffraction angles <60° is also acceptable. Figure III.13. shows the contrast for each fringe as a function of a diffraction angle from the mask grating. Two different combinations of the polarisation angles are shown. One is for θ_r=29° and θ_o=-56° (Fig. III.13.a)) and the other is for θ_r=39° and θ_o=-45° (Fig. III.13.b)). The contrasts of the interference fringes made with the incoming reference beam (the reflection holograms: thick lines) are all lower than those with the TIR beam (the transmission hologram: thin lines). The contrasts for the transmission holograms of Fig. III.13.b) are higher than those for Fig. III.13.a). This is expected from Fig. III.8.

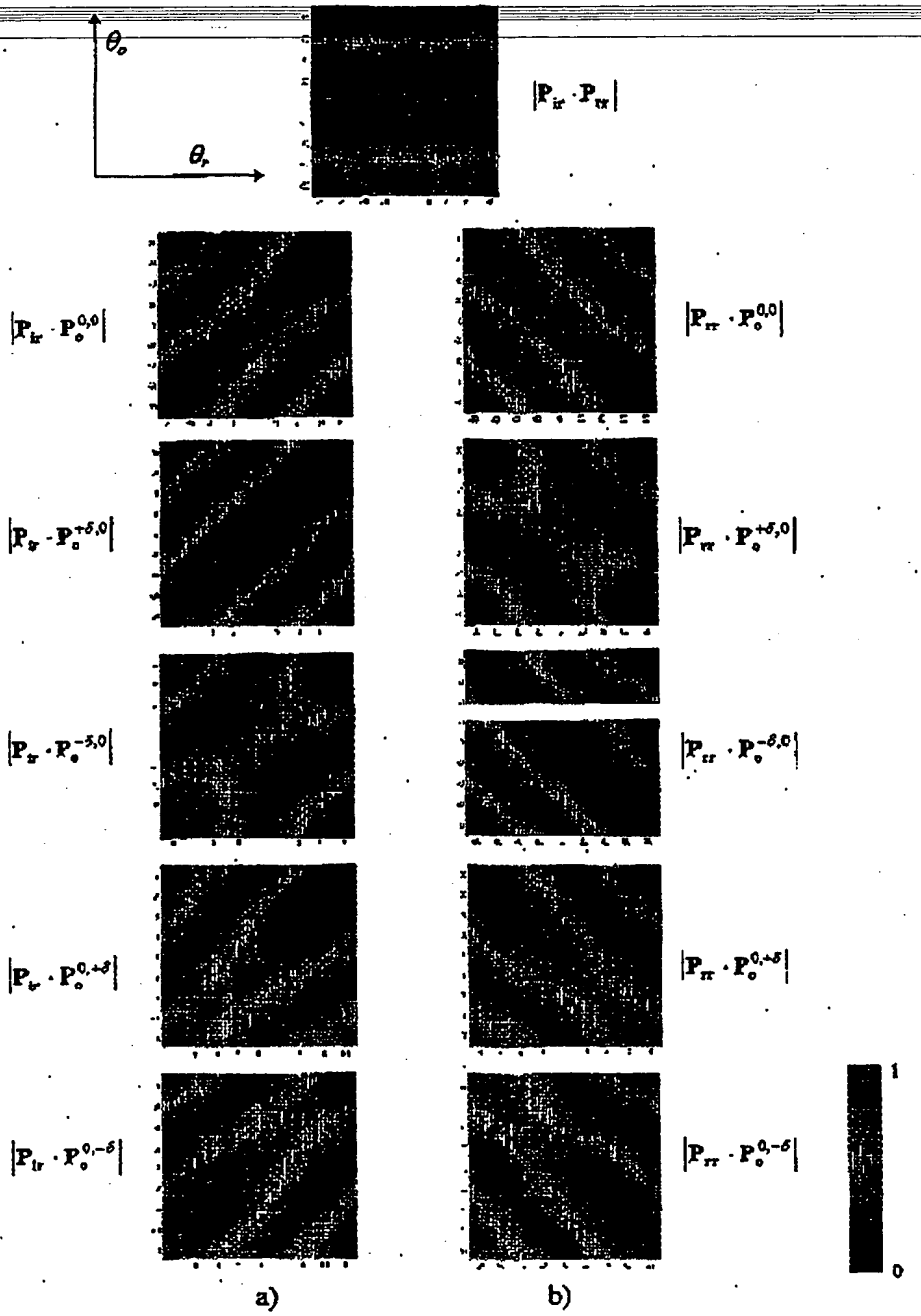

Fig. III.12. Contrast as a function of θ_r and θ_o for different holograms formed by different polarisation combinations. The diffraction angle from the mask is assumed to be 60°: a) interference between incoming reference beam and diffracted object orders. b) interference between TIR beam and diffracted object orders.

In Fig. III.13.b), the angular dependence of the contrast for the transmission hologram formed with -1st order in the x-axis and +1st order in the y-axis shows a perfect superposition on top of each other as that with +1st in x and -1st in y does the same. For the reflection hologram, the contrasts of +/-1st order in the x-axis are the same as those of +/-1st order in y-axis. This is possible because of the common polarisation angle of θ_o =-45°.

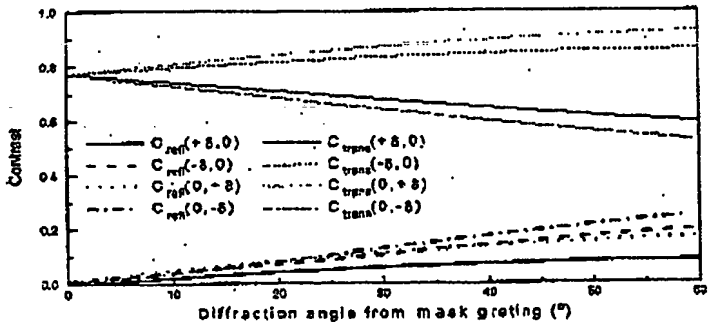

a)

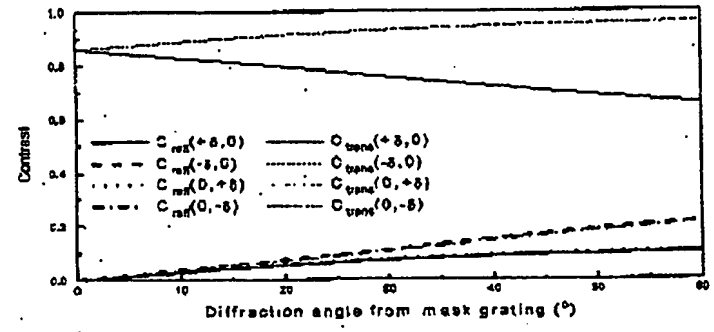

b)

Fig. III.13. Contrast as a function of diffraction angles from the mask for each hologram. The polarisation angles for the reference and the object beams are: a) θ_r=29° and θ_o=-56°, b) θ_r=39° and θ_o=-45°.

$$C_{refl}(+\delta,0) = \left|\mathbf{P}_{tr}\cdot\mathbf{P}_{o}^{+\delta,0}\right| \qquad C_{trans}(+\delta,0) = \left|\mathbf{P}_{rr}\cdot\mathbf{P}_{o}^{+\delta,0}\right|$$

$$C_{refl}(-\delta,0) = \left|\mathbf{P}_{tr}\cdot\mathbf{P}_{o}^{-\delta,0}\right| \qquad C_{trans}(-\delta,0) = \left|\mathbf{P}_{rr}\cdot\mathbf{P}_{o}^{-\delta,0}\right|$$

$$C_{refl}(0,+\delta) = \left|\mathbf{P}_{tr}\cdot\mathbf{P}_{o}^{0,+\delta}\right| \qquad C_{trans}(0,+\delta) = \left|\mathbf{P}_{rr}\cdot\mathbf{P}_{o}^{0,+\delta}\right|$$

$$C_{refl}(0,-\delta) = \left|\mathbf{P}_{tr}\cdot\mathbf{P}_{o}^{0,-\delta}\right| \qquad C_{trans}(0,-\delta) = \left|\mathbf{P}_{rr}\cdot\mathbf{P}_{o}^{0,-\delta}\right|$$

As is expected, the separation between the two contrast groups increases as the diffraction angle decreases. This means that the relative strength of the transmission hologram over the reflection hologram increases as the diffraction angle decreases. For masks having gratings in both x- and y-directions, the optimum polarisation combination is θ_r=39° and θ_o=-45°.

III.1.2.2. Effect of beam intensity ratio

If a photomask is employed in the object beam path, multiple diffraction orders are involved in interference fringe formation. In this case, the amplitude of each diffraction order will be different from each other. To form fringes in the recording material for weak diffraction orders, the fringe intensity should be higher than E_0 in the γ-curve. If these fringes result in a too shallow surface modulation depth, the diffraction efficiency from them during reconstruction is also too weak. If the γ-curve is too steep, fringes from small features might not be recorded, while those from large ones are saturated. Since the fringe contrast in the hologram is a function of amplitude ratio between beams, this ratio should be chosen such that interference fringes from big features as well as from small ones can be recorded simultaneously.

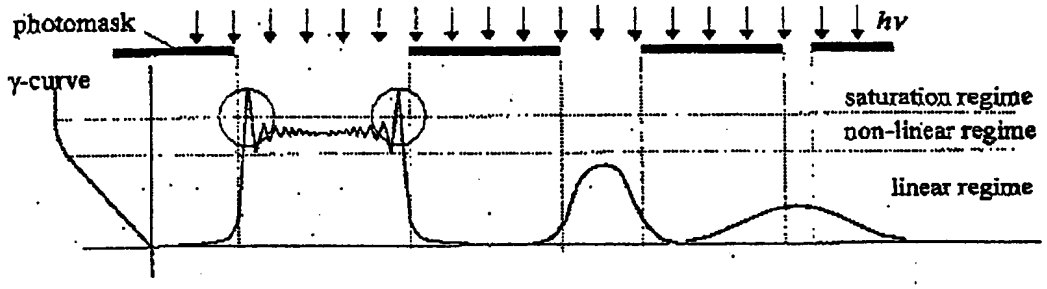

Fig. III.14. Three different feature sizes and their images.
Fresnel fringes caused by a large feature can fall in the non-linear and the saturation regimes of the contrast curve.

Figure III.14. illustrates the image difference between large and small features. The image with a large feature has Fresnel fringes having high intensities at the edge, while that with a small one has a widely spread image. Because photoresists in general have a non-linear response (see Fig. II.5), we may have unwanted results. Even though the SNR240 resist has a very low γ-value (γ=1.2), the Fresnel fringes may exceed the linear regime of the γ-curve. Accordingly, they will be nonlinearly recorded. In this case, the information corresponding to the Fresnel fringes is missing, resulting in side-lobes along the large features.

To have a controlled intensity change over the hologram material, we use a knife-edge mask in the object beam path. The beam intensity behind this mask will oscillate in the clear area and monotonically decrease in the shadow area. The gap between the mask and the hologram surface is set to 125μm. If we reduce the object beam intensity with respect to the reference beam, the intensity of the Fresnel fringe can fall in the linear region of the γ-curve. In this case, the fringe contrast can also be modified. Figure III.15. shows calculated and AFM-scanned Fresnel fringes for the intensity ratio between the object and the reference beams of 1:1 and 1:4. The fundamental gratings are formed within the envelope between the maximum (I_{max}) and the minimum intensities (I_{min}) of the calculated curves. Compared to the beam intensity ratio of 1:1, I_{max} of the beam intensity ratio of 1:4 is decreased, while I_{min} is increased. This results in a small envelope. The fundamental gratings for the 1:4 ratio fill the envelope more faithfully than those for the 1:1 do. The poor fidelity at high peaks of 1:1 ratio is as a result of the nonlinear recording. The peak intensity of I_{max} is noticeably decreased with 1:4 ratio. Therefore, the peaks must fall within the linear zone.

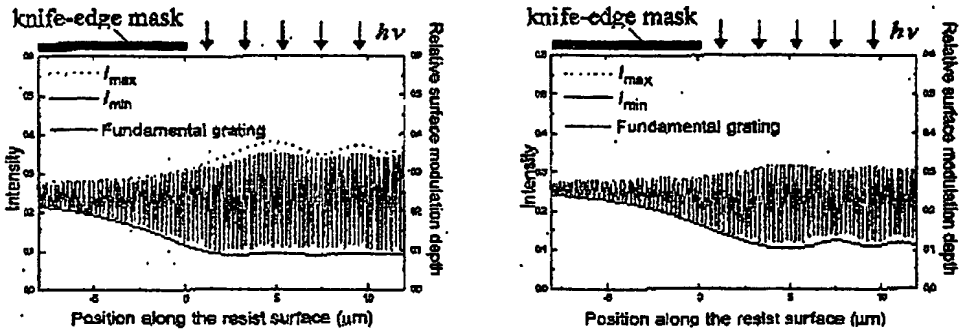

Fig. III.15. Fresnel fringes formed with a knife edge mask 125μm above the resist surface: a) calculated fringe (an envelope) and AFM-scanned profile (a high frequency grating) for the beam intensity ratio (object : reference) 1:1. b) same as a) but for the 1:4 beam intensity ratio.

To record fringes from large and small features simultaneously for the γ-value of 1.2, the beam intensity ratio of 1:4 between the object and the reference beams is acceptable.

III.1.3. Summary

The intensity distribution within the hologram material is governed by the polarisation combination between the object and the reference beams. The polarisation combination is chosen to maximise the contrast of the transmission hologram. It is important to consider the feature orientation on a mask in choosing a polarisation combination. For this requirement, the polarisation angles of -45° and 39° for the object and the reference are chosen and shown to be optimal.

The fringe contrast in combination with the recording linearity is affected by the beam intensity ratio between the object and the reference beams. Experimental and theoretical results show that the beam intensity ratio of 1:4 is the best choice for the process used.

III.2. Diffraction efficiency

It is useful to correlate the surface modulation depth with the diffraction efficiency. Since a transmitted first order diffraction beam contributes to image formation during reconstruction, the efficiency of this order is of interest. Figure III.16. gives a schematic representation of the possible diffraction orders associated with the grating. If the grating is made with the 0th order object beam and the reference beam, a fundamental grating period of 242.8nm (231nm within the resist) will be formed on the resist surface. Since this grating period has a deep modulation, the diffraction efficiency is studied with this order only. For this grating period, if there are any reflected diffraction orders which hold a high efficiency, these orders shouldn't reflect back to the grating again. Fortunately, the first two orders (0th and 1st) are reflected towards either one or two absorbers attached to the prism, and the 2nd order beam heads towards the incident beam. Therefore, only the transmitting 1st order leaves the grating towards the wafer surface.

The transmitted 1st order diffraction efficiency depends on the grating form and depth. This is already covered in a number of references[6-9]. We use a coupled wave theory to calculate the diffraction efficiency[9,10]. In our case, the beam is incident at 45° from a fused silica substrate (n=1.5 at λ=257nm) which sits on the prism with a matching fluid in between. The polarisation used for the calculation and the measurement is S-polarisation (perpendicular to the plane of incidence). No photomask is used.

The dependence of the diffraction efficiency is shown in Fig. III.17. for various diffraction orders. The grating shape for the calculation is considered to be similar to Fig. III.10. The grating shape is digitised and is divided into 50 horizontal slabs for the diffraction efficiency computation. A number of specimens are prepared with different exposure doses and development times to give different modulation depths. The specimens that have a 1:1 duty ratio are chosen for the diffraction efficiency measurement.

The transmitting 1st order wave intensity is low for low depth, while the reflecting 0th order (TIR) is very high. As the grating depth increases, the efficiency increases until the depth reaches ~80nm and then decreases with an oscillating behaviour. For a depth of ~180nm, the transmitting 1st order efficiency becomes almost zero, while the reflecting 2nd order reaches a maximum value as high as 74%. The maximum obtainable efficiency for the transmitting 1st order is ~36%. This is confirmed experimentally for ten different depths as plotted with open squares in the figure. The experimental result is in excellent agreement with the simulation result.

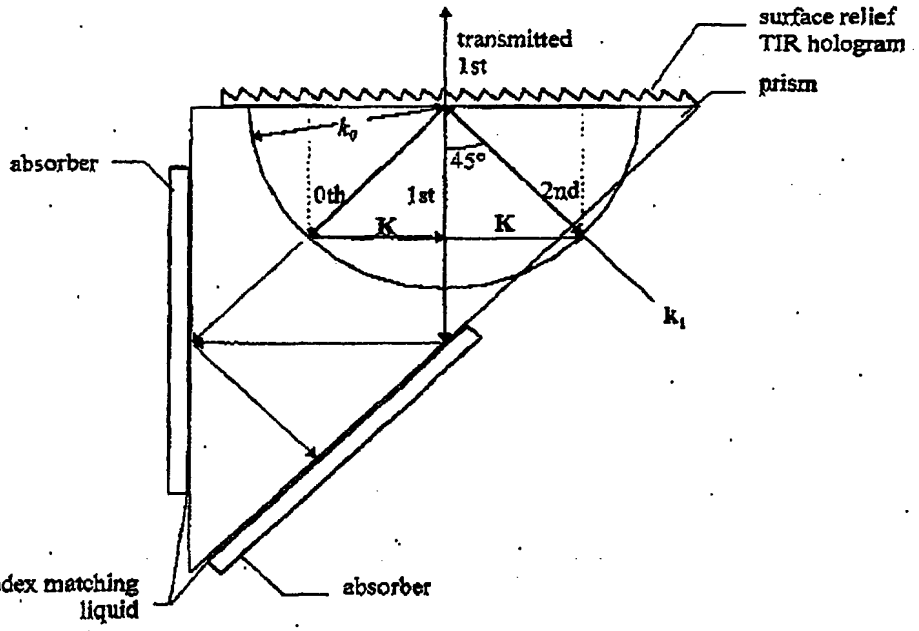

Fig. III.16. Transmitting and reflecting wave vectors. The first two reflected diffraction orders are absorbed by the absorbers, while the 2nd order beam is reflected towards the incidence beam.

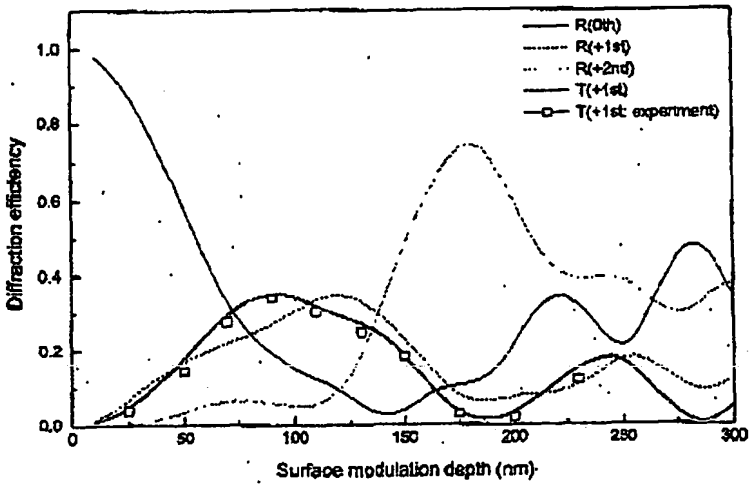

Fig. III.17. Diffraction efficiency as a function of the surface modulation depth for various diffraction orders. The maximum transmitting 1st order diffraction efficiency reaches ~36% at the depth of ~80nm.

If all the parameters chosen in the previous section were used, the modulation depth wouldn't exceed 70nm. The depth might be between 30nm and 50nm depending on the development conditions to suppress the scattering. The scattering problem is studied in the next chapter. In this case, the efficiency will be only in the range of 5%-10%.

References

1. Karl A. Stetson, "Improved resolution and signal-to-noise ratios in total internal reflection holograms", *Appl. Phys. Lett.*, 12, 362-364, June. (1968).
2. J. Brook and R. Dändliker, "Holographic photolithography for submicron VLSI structures", *Microelectron. Eng.*, 11, 127-131 (1990).
3. Francis Clube, Simon Gay, Denis Struchen, Jean-Claude Tisserand, Stephane Malfoy, and Yves Darbellay, "HOLOGRAPHIC MICROLITHOGRAPHY", *Optical Engineering*, 34, 2724-2730 (1995).

4. F.S.M. Clube, "Holographic Microlithography", *Diffractive Optics*, 391-418 (1997)Akademie Verlag, Berlin.
5. Wayne M. Moreau, *SEMICONDUCTOR LITHOGRAPHY*, 312-321, (1988) Plenum Press, New York.
6. S.T. Peng, H.L. Bertoni, and T. Tamir, "Analysis of periodic thin-film structures with rectangular profiles", *Opt. Commun.*, 10(1), Jan.(1974).
7. R.H. Morf, "Exponentially convergent and numerically efficient solution of Maxwell's equations for lamellar gratings", *J. Opt. Soc. Am. A*, 12(5), 1043-1056, May (1995).
8. K. Knop, "Rigorous diffraction theory for transmission phase gratings with deep rectangular grooves", *J. Opt. Soc. Am. A*, 68(9), 1206-1210, Sep. (1978).
9. M.G. Moharam and T.K. Gaylord, "Diffraction analysis of dielectric surface-relief gratings", *J. Opt. Soc. Am.*, 72(10), 1385-11392, Oct. (1982).
10. R.R.A. Syms, *Practical Volume Holography*, 344 (1990), Clarendon express, Oxford.

Because a transparent resist delivers more scattered light than an absorbing one, as long as the molecular structure, solvent content, etc. stay the same, the thickness should be limited. Even if the scattering intensity with an absorbing resist is low, it weakens the fringe visibility. However, the scattering level with a thin resist doesn't seem to be very low for its thickness. Figure IV.6. indicates the reason. The intensity within the resist has a standing wave pattern that corresponds to a Lippmann hologram for the TIR holography. The standing wave ratio is higher with a thin resist than with a thick one because of transparency. Therefore, the scattering generated in the high intensity regions increase. For very thin resists, the high intensity regions dominate.

In summary, thick resists are not desirable because of high scattering as well as poor fringe visibility. But thin resist should also be avoided, because of defects within the resist and poor etch resistance.

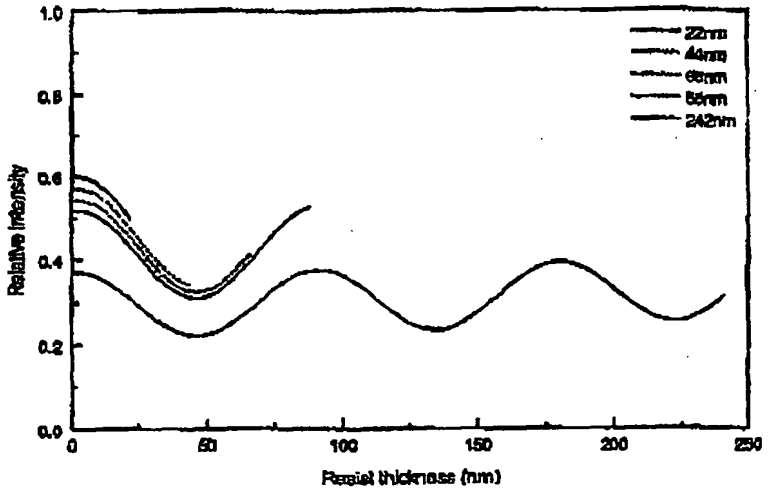

Fig. IV.6. Standing wave curves for SNR240 resist with five different resist thicknesses.

IV.1.2.3. Solvent content effect

The base-resin molecule and the photo-acid generator (PAG) act as scattering sources, but resist solvents may also cause scattering. Normally solvents are evaporated during spinning of the chuck.

The amount of retaining solvent after spinning is a function of spin-speed. But the spin-speed again affects the resist thickness. Therefore, the spin-speed should be constant to reduce the number of experiments. Even after spinning, the resist still contains solvent in the range of 10-20% by weight[15]. The amount of solvent is reduced to less than ~5% in the prebaking cycle. Higher prebake temperature would reduce the solvent content to ~1%. But in this case, the characteristics of the resist completely changes whereby the photosensitivity is reduced. Residues also can be formed. For these reasons, the prebake temperature should be chosen within the temperature range that does not significantly affect the resist characteristics.

IV.1.2.3.1. Prebake effect

A number of fused silica substrates are coated with SNR240 resist at different spin-speeds. Since the thickness of resist also changes with prebake temperatures, the thickness should be constant for all these temperatures to maintain the standing wave distribution. After coating, the resist coated substrates undergo a prebake for 60s with different temperature settings. Six different temperatures are chosen within the recommended temperature range, 100°C-135°C[16]. In addition to this temperature range, we also use temperature settings such as 23°C and 90°C for the low end and 140°C and 150°C for the high end.

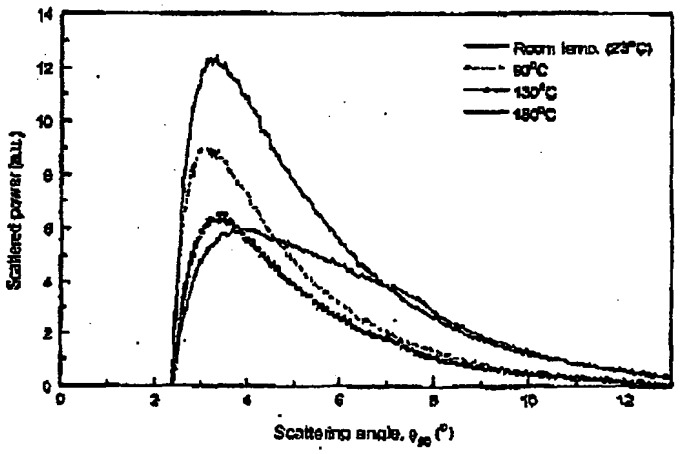

Fig. IV.7. Scattered power as a function of scattering angle for four different prebake temperatures. The highest scattering is found at the room temperature, while the lowest one is observed at 130°C. The prebake time:60s for each temperature.

Figure IV.7. shows the scattering distribution as a function of scattering angle (θ_{sa}) within the resist. Prebaking at room temperature (23°C) causes a lot of scattering compared to the other temperatures. Because the prebake temperature affects the solvent content within the resist layer, prebaking at room temperature does not fully evaporate the residual solvent. Once the resist film is baked at temperatures higher than room temperature, we observe that the scattering level decreases rapidly. The prebake temperature of 130°C results in the lowest scattering level. We observe that the scattering level increases again at 140°C (not shown in Fig. IV.7.). At this high temperature, the base resin and the PAG thermally react with each other [17] resulting in a large molecular weight and therefore increase scattering. A lower scattering level is observed with even higher temperatures like >150°C. At these temperatures of 140°C-150°C, the reaction between the base resin and the PAG may cause a complete polymerisation that darkens the resist. The scattered light is then strongly absorbed by the resist film.

If the residual solvent content affects the scattering level, how can we further remove it? It may be possible to reduce the solvent content by slowly heating up the resist film. The heat-up acceleration is adjusted by employing different electric powers to the hot plate together with an additional aluminium plate to slow the heating. The temperature is measured with a thermocouple attached to a wafer that is placed on the hot plate.

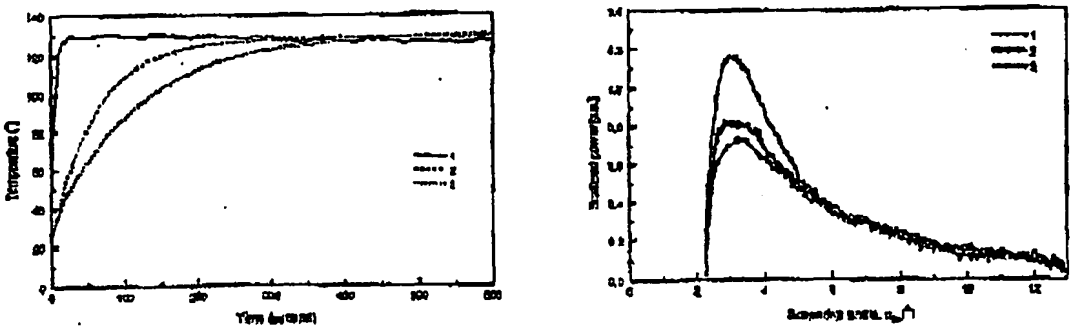

a) b)

Fig. IV.8. Temperature rise as a function of a) time and b) corresponding scattering levels.

Figure IV.8.a) shows the temperature rise as a function of time for three different heat cycles. Curve 1 corresponds to the normal condition for all our experiments made until now. The temperature is set to 130°C because the lowest scattering level has been reported in Fig. IV.7. The scattering level for fast heating cycles is higher than that of slower ones as shown in Fig. IV.8.b). Slow heating permits the residual solvent to leave the resist skin very gently and steadily. But the difference between the dependence 2 and 3 is small. Therefore, the dependence 2 is preferred for faster process time.

IV.1.2.3.2. Dilution effect

The role of the resist thickness is very important to control the fringe contrast, defect density, etch resistance, scattering, etc. The resist thickness (250nm) for our experiment is chosen to satisfy these requirements. Resists normally consist of 3 or 4 components such as a base resin, a sensitiser, a solvent[18], and a cross-linker for a negative resist. The components are solids except for the solvent. Because these solids are dissolved in the solvent, the solid content in a resist depends on the dilution of the resist. The resist thickness, T_{pr}, depends on three different parameters[19].

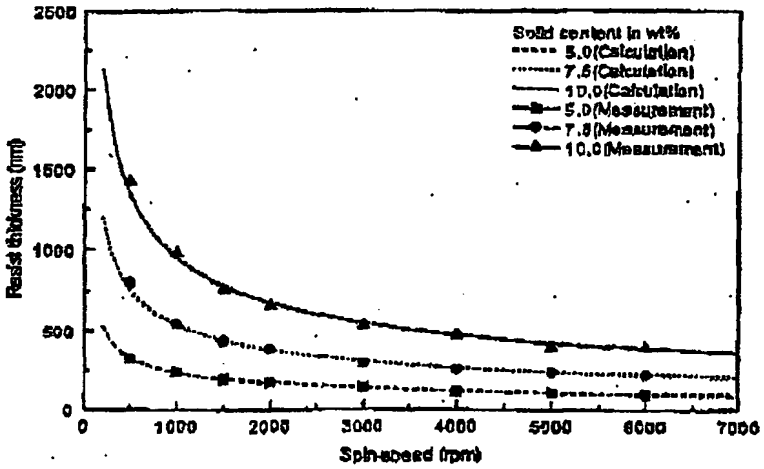

Fig. IV.9. SNR240 resist thickness as a function of spin-speed for various solid contents.

$$T_{pr} = K\frac{P^2}{\sqrt{W}}, \qquad \text{(IV.2)}$$

where K is th spinner constant, P is the perc ntage of solids in the resist, and W is the spin-speed in rpm/1000. If we use a dedicated spinner and a fixed resist, the resist thickness is solely a function

of the spin-speed. According to eq. (IV.2), the resist thickness is affected by the solvent content change more strongly than by the other two parameters.

Figure IV.9. shows the resist thickness as a function of the spin-speed for three different solid concentrations for the SNR240 resist. With a concentration of 10wt%, it is impossible to obtain a resist thickness of 250nm by varying the spin-speed between 2000-6000rpm. If the resist is diluted from 10wt% to 7.5wt% in solid content, a thickness of 250nm is obtained at 4000rpm. Therefore, dilution permits us to control thin resist thicknesses at reasonable spin-speeds.

Because there is no common thickness for these three dilution with a spin-speed between 2000rpm and 6000rpm, we consider a lower spin-speed for a lower resist concentration. It is possible to obtain a common thickness of 400nm if we are at 5000rpm for the 10wt%, 1500rpm for the 7.5wt%, and 300rpm for the 5.0wt%. The thickness uniformity with 300rpm and 1500rpm shows 5% and 2.5% respectively across the 2 inch diameter substrate, while that with 5000rpm is ~1%. But the thickness variation at the center of the substrate is less than 1% for all these spin-speeds.

The scattering level is compared among three different solid contents in Fig. IV.10. The prebake temperature is set to 130°C for 5 minutes. A small solid content gives rise to a high scattering level even for the optimum prebake condition. This means that it is not possible to completely eliminate the solvent within the resist film at low resist concentration. The absolute solvent content, therefore, should be kept as small as possible.

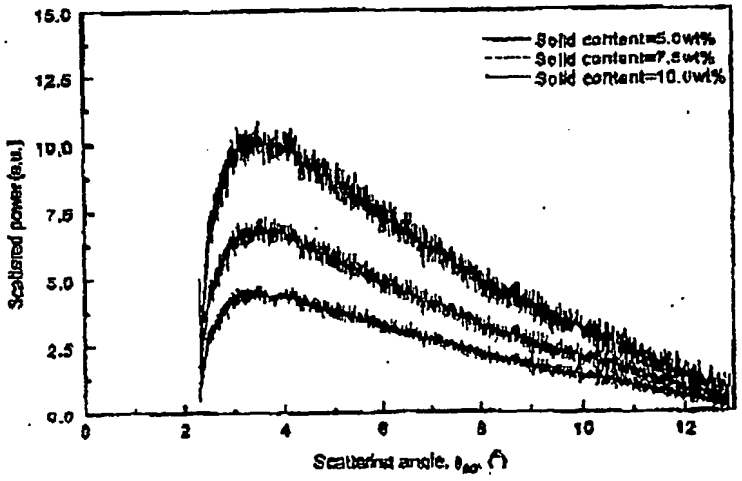

Fig. IV.10. Scattering comparison of three different solid contents. The spin-speed is adjusted to achiev a common thickness of 400nm. Low concentration resist gives rise to increasing scattering.

By changing only the spin-speed, however, the resist thickness cannot be reduced by a factor of two from its original bottle having a high solid content. In this case, we adjust another parameter, K, in eq. (IV.2). This parameter may be related to factors influencing the solvent evaporation conditions such as the atmospheric pressure, the humidity, the ambient temperature, etc. In our laboratory which is not equipped for controlling the environment, we observe a significant thickness fluctuation depending on weather conditions. Therefore, we made a simple apparatus with which we are free from environmental conditions.

Figure IV.11. shows the chuck types that we use for our experiments. One is the conventional chuck and the other is a closed chuck. The closed chuck is designed to keep most of the evaporated solvent within the volume and to let small amount of solvent out through small holes (dia. 0.5mm) around the chuck wall. With the conventional chuck, the solvent of the resist applied on the substrate evaporates easily during spinning because the resist is exposed to the air. But with the closed chuck, the solvent cannot easily escape from the chuck. Since the lid is closed after resist application onto the substrate, the solvent evaporated from the resist, saturates the volume of the chuck. Under the saturated environment, the resist does not quickly dry during spinning. This slow drying results in thin resist thickness.

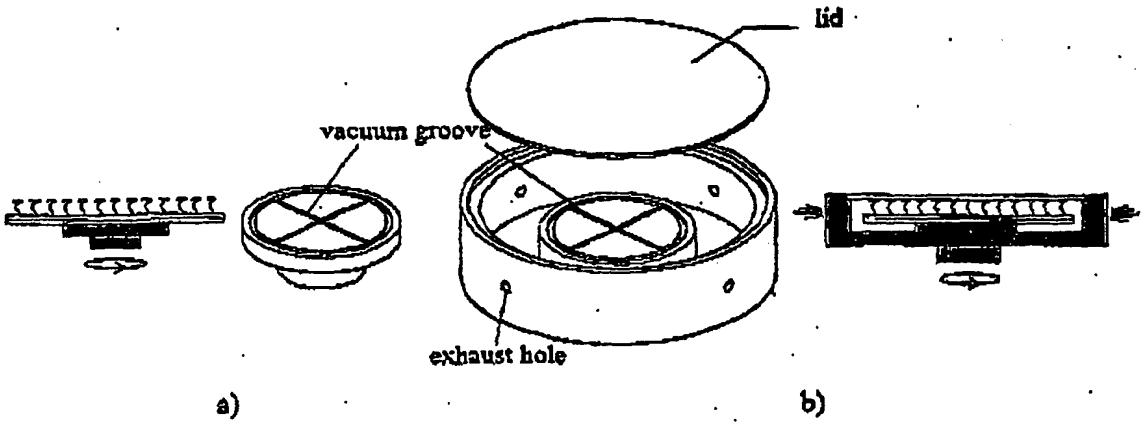

Fig. IV.11. Spinner chuck types of cross-sectional and bird's eye views.
a) Conventional chuck b) Closed chuck

The solvent evaporation is noticeable with the closed chuck only when the transparent lid is opened after spinning. The color of the resist film changes as soon as the lid is opened. This means that the resist thickness changes with solvent evaporation. But such a color change is already observable during spinning with the conventional chuck. This means that the resist surface with the conventional chuck is hardened during spinning. This "hard skin" formed with the conventional chuck may block the solvent evaporation from the resist film. But the resist surface with the closed chuck is soft because it is dried with an ambient solution atmosphere.

The solvent evaporation rate may be changed depending on the volume of the chuck. A cylindrical lid is used to adjust the volume of the chuck. Since the spinner constant (K) is closely related to the ambient, the chuck volume permits to control the spinner constants.

The resist thickness as a function of spin-speed for different spinner constants is given in Fig. IV.12. The spinner constants are obtained by fitting the measured thickness. This figure shows that the resist thickness can easily be adjusted by changing the chuck volume without adding any solvent. It is not possible to obtain 250nm resist thickness with the conventional chuck of K=93. To obtain a thickness of 250nm, 5300rpm, 2400rpm, and 1000rpm are K-values of 60, 41, and 24, respectively. For the most uniform coating, 2400rpm with K=41 is chosen.

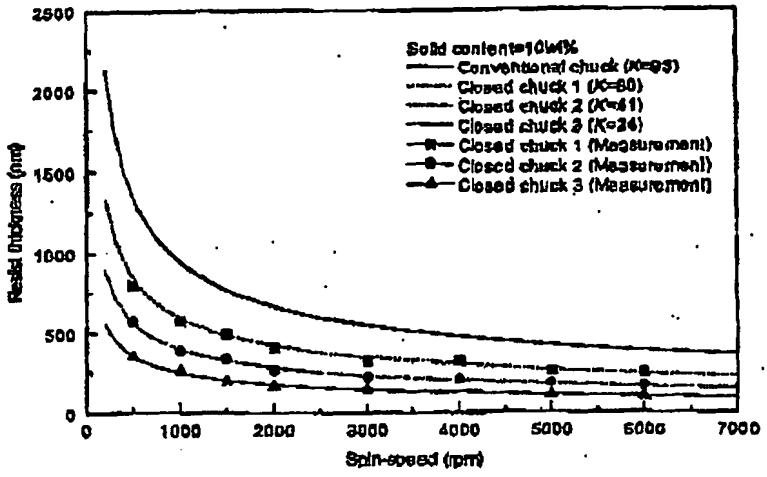

Fig. IV.12. Resist thickness as a function of spin-speed for different chuck volume corresponding to different spinner constants (K). The change of the chuck volume leads to different thickness curves.

The scattering level for the two different chuck types is shown in Fig. IV.13. Figure IV.13.b) is the total scattering corresponding to the area under each curve in Fig. IV.13.a). The thickness is changed by varying the spin-speed for both of the chucks. There is a big difference between the conventional and the closed chucks. The scattering levels strongly depend on the spinner constant K. The scattering with the closed chuck of K=41 is very much decreased by a factor of ~3. The reason for this may be that the absolute solvent content in the resist liquid is small and that the solvent in the film must completely be evaporated during prebaking at 130°C through the "soft skin".

We have also verified the proportionality of the scattering level to the K-values. More scattering results from higher K-values at a given concentration. Since high K-values are associated with quick solvent evaporation, the resist surface dries quickly. This dried skin may partially block the under-skin-solvent evaporation during both the spinning and the prebake. Therefore, the saturated ambient during coating process is desirable to leave a "soft skin" through which the under-skin-solvent penetrates easily during the prebake step.

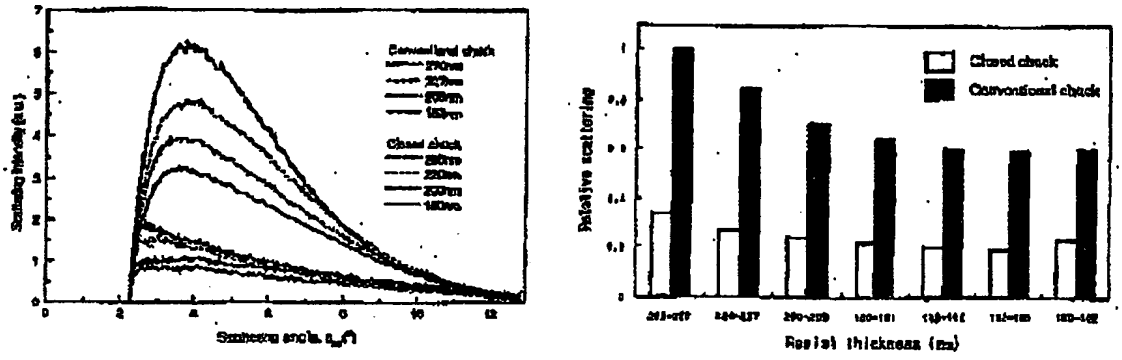

a) b)

Fig. IV.13. Comparison of scattering level between two different chuck types for different r sist thicknesses. The spinner constants for the closed and the conventional chucks are K=41 and K=93, respectively.
a) Scattering intensity vs. scattering angle. b) Relative scattering vs. resist thickness.

IV.2. Scattering after processing

Until now we have explored the scattering generated from a virgin resist that affects the fringe quality during recording and adds to the scattering generated after development. Since the reconstruction quality is affected by the total scattering, the scattering from the processed resists is also important. Because the surface roughness can be considered to have random period in random orientation, the incident beam is diffracted randomly. Therefore, the surface should be smooth to avoid such scattering. But it is difficult to achieve a smooth surface after processing, because the developer reveals defects such as voids, various molecular sizes, etc. hidden under the resist skin.

During development, the resist surface is attacked by the developer liquid. The surface quality after quenching with water does not tend to be microscopically homogeneous because the resist solubility in the developer is not constant through the resist depth. But such roughness may be improved with a "mild" process. This mild process can be accomplished by optimising the effects due to development time, developer concentration, and developer temperature.

IV.2.1. Development time and developer concentration

It is necessary to know the cause of the rough surface for scattering suppression after processing. There are two possible causes: one is the molecular weight distribution within the resist, and another one is the formation of voids in the resist layer during the coating and the prebaking steps. The molecules of the resist consisting of a base resin, a PAG, and a cross-linker, are randomly distributed. Each component has a different spectrum of molecular weights (MW=5,000-15,000). The developer dissolves uncross-linked or loosely-linked molecules. The molecules with different molecular weights are revealed through rough surfaces. Because the solvent is evaporated from spaces between the molecules, voids may be left behind. Most of these voids can be refilled with the resist molecules during the annealing period of the prebaking cycle. But voids remain that act as scattering centers during the recording period. The developer liquid easily penetrates across these voids that give rise to a rough surface.

Figure IV.14. illustrates the roughness evolution with development time for a "harsh" and a "mild" processes. A harsh and a mild processes are qualitatively defined as the processes that the developer attacks the resist harshly and mildly, respectively. The developer attacks the resist both vertically and horizontally. As the development time increases, the unexposed area is more quickly dissolved than the exposed area. But even the exposed area is also eroded by long development time. The

seriousness of such erosions is different between the harsh and the mild processes. If a harsh process is used, rough surfaces may result because only strongly cross-linked molecules remain with missing molecules (lightly cross-linked ones) around. The developer also quickly penetrates across the voids lifting up underlying molecules. If a mild process is employed, even lightly cross-linked molecules are not washed away and the development across voids would not be effective. Therefore, a smooth surface will result.

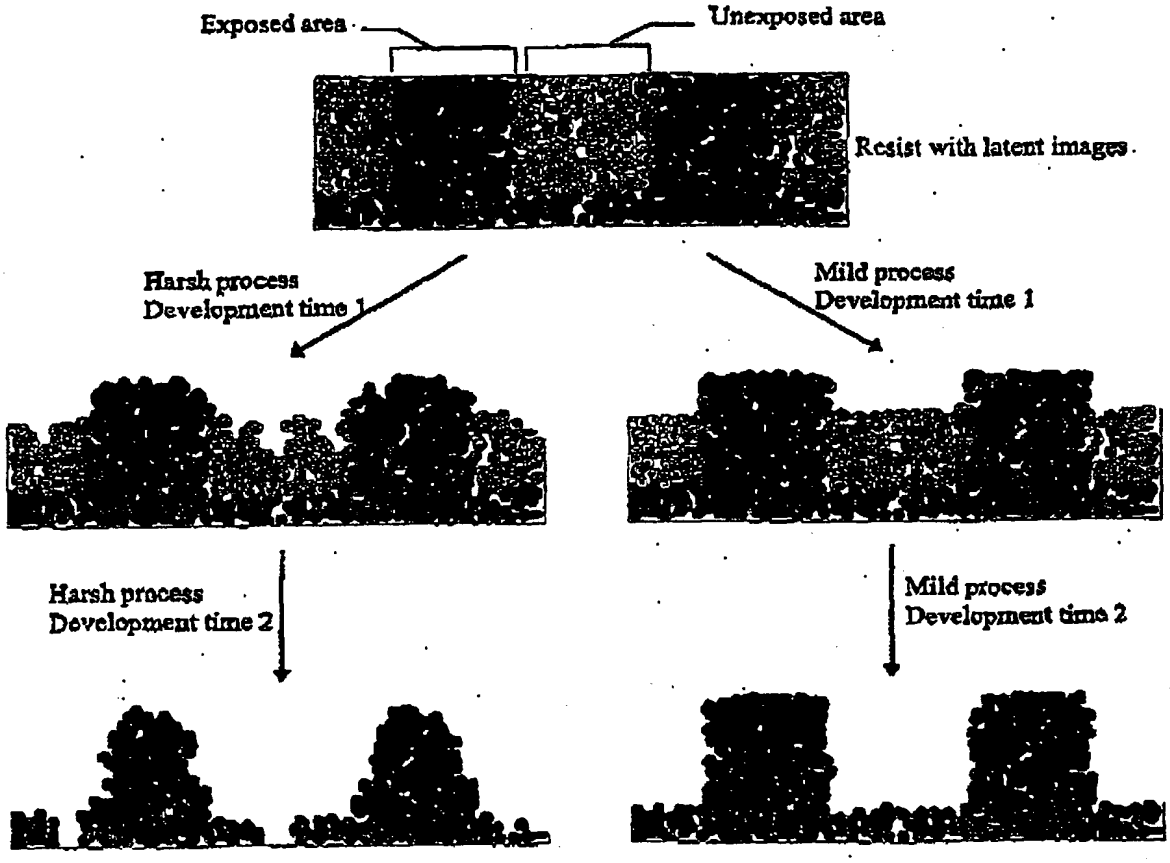

Fig. IV.14. Illustration of roughness evolution with development time for harsh and mild processes. A smooth surface may result with a mild process, while a rough surface is unavoidable with a harsh process.

The harsh and the mild processes are determined by the roughness. They depend on the development time, the developer concentration, and the temperature of the developer liquid. The harsh process may be the combination of a long development time, a strong developer concentration, and a high

temperature of the developer liquid. The two factors that predominantly determine the development speed are the development concentration and the temperature of the developer. The development time is determined by the soaking time of the resist in the developer liquid.

If a resist coated substrate is immersed in a developer liquid for a long time, the liquid that first reaches the substrate after penetrating through the short cut (e.g. voids, pinholes, etc.) will also penetrate laterally along the substrate. This lateral penetration lifts up the adjacent area or leaves a swollen area behind that again will generate strong scattering. If only a short period of time is assigned for development, the liquid cannot reach the substrate to peel off the neighbouring area.

Figure IV.15. represents AFM images showing the roughness evolution with development time. The resist thickness is 250nm at the prebake temperature of 130°C. This resist is exposed at 30mJ/cm^2. The high exposure density avoids a complete "wash-out" after 25s development time with the developer dilution to water of 4:1. Even the virgin resist shows a lot of voids about 2-10nm in diameter. These defects seem to exist within the bulk as well as the surface. They are presumably generated by micro-bubbles in the resist. These bubbles may contain water, air, and/or solvent gases that are evaporated at different rate during spinning. This virgin resist reveals enlarged holes and a rough surface after 10s of development time. Further development uncovers the surface roughness and enlarges the holes all over the layer. The rough surface after development is definitely a cause of the scattering.

The results of more elaborated experiments are given in Fig. IV.16. The closed chuck of Fig. IV.11.b) is used for this experiment. The exposure dose as well as the development time and the developer concentration are varied. The exposure time (ET1 to ET6) is determined by the condition that the remaining resist after each development is 10, 20, 40, 60, 80, and 100% of the nominal thickness of 250nm. In this fashion, any difference caused by a residual thickness variation can be avoided. The development time is varied from 10s to 25s with 5s increment. The dilution ratio of the MF322 developer with water is 1:1 and 2:1 by volume. Each specimen is scanned by AFM. The scan area is 2.5μm x 2.5μm.

The 2:1 dilution ratio generally shows worse roughness than the 1:1 ratio. The strong developer concentration must attack the resist surface harshly. We find the longer development time the worse the roughness. Swelling through loosely bound molecules and voids must generate rough surfaces as illustrated in Fig. IV.15.

IV. Scattering

Scattering is one of the most disturbing problems in our experiments. Scattering from a gelatine hologram material using a silver halide is well known[1-3]. People who have used such a material claim that the scattering problem will disappear when using a photopolymer or a photoresist[4]. This may be true if they are used at long wavelengths (λ>364nm). Because the flux density of the scattering light is inversely proportional to the fourth power of the wavelength[5-8,10], the degree of scattering becomes very high as the wavelength decreases.

Scattering superimposes all the reconstructed images. For shallow surface modulation, the scattering is not negligible compared to the diffraction efficiency. In chapter III, we studied the enhancement of the surface modulation by changing both optical and resist factors. All the parameters such as absorption, refractive index, resist thickness, polarisation, and beam intensity ratio are tuned to eventually increase the surface modulation for masked TIR holography. However, all these parameters are not optimised from the scattering point of view. We have found a high scattering level even with these parameters.

To enhance the signal to noise (S/N) ratio, we must either improve the signal level or reduce the noise level, or both. In this chapter we explore the S/N ratio improvement by reducing the noise level through extensive experiments.

IV.1. Scattering during recording

We observe a lot of noise in the reconstructed images. From both the material and the process point of view, we examine all potential factors that cause noise. Surprisingly, we observe a noticeable scattering level during recording as well as during reconstruction. This implies that the flat resist layer of SNR240 is inhomogeneous. But the scattering level during recording is not as high as that during reconstruction after processing. Since the signal level with shallow modulation is comparable to the scattering level, it is better to suppress this noise contribution as much as possible.

If there are scattering centres within the resist layer, they may remain even after processing. Therefore, the scattering signal that destroys the reconstructed images, is the result of the scattering centres created before and after processing. If there is scattering during recording, scattering gratings might result[4,9]. Therefore, we need to examine the origins of the scattering associated with a virgin layer of resist. We examine other resists as well as SNR240 to compare the scattering characteristics.

With increasing exposure dose, the remaining thickness increases and the roughness decreases. Because SNR240 is a negative resist, the exposed area remains after development. A low exposure dose does not bind the molecules strongly. On the other hand, high exposure dose binds them strongly and causes fewer loosely bound molecules. The rms roughness values in nm obtained from AFM scans are written on top of each scanned image.

If only 5nm roughness corresponding to 10% of the modulation depth (50nm) is considered to be acceptable, the dilution ratio of 2:1 should be discarded. Since the modulation depth of the grating is ~50nm corresponding to 20% of the nominal thickness, the roughness of the grating corresponds to the exposure doses of ET5 and ET6. in Fig. IV.16. For these two exposure doses plus the acceptable roughness of 5nm, the development times of 10 and 20s are acceptable for the 1:1 dilution ratio.

IV.2.2. Developer temperature

To suppress the surface roughness, a slow and gentle development is considered. In general, the developer temperature is not very much different from the ambient temperature such as 23°C. However, only a few researchers have worked on the effect of the low developer temperature[20].

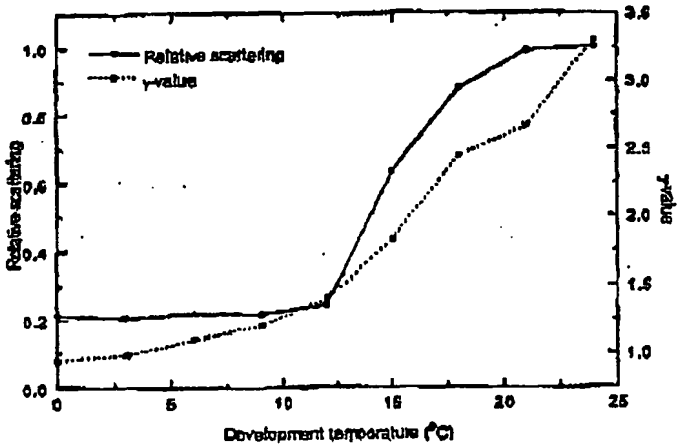

Fig. IV.17. Relative scattering level and γ-value as a function of development temperature. The scattering level jumps at ~12°C and the γ-value also increases rapidly from there.

But they only investigated contrast changes or photospeed changes as a function of the developer temperature. The surface roughness was not their concern. It is known that the developer speed as well as the contrast changes considerably with the developer temperature. Therefore, the developer temperature is usually room temperature.

We vary the developer temperature from 0°C to 24°C to observe the effect on the roughness and the contrast. Figure IV.17. shows the results. The relative scattering level remains low at temperatures below 12°C. It rapidly increases for temperatures >12°C. The binding energy between the molecules below 12°C may detain the molecule from being washed away by the thermally less activated developer. As soon as the temperature reaches 12°C, the binding energy gives way to the activated developer resulting in a rapid development rate. This high development rate causes a rough surface as other factor such as a strong developer concentration does.

We also observe a continuous increase in the γ-value with increasing developer temperature. It is encouraging that we can change the material linearity only by changing the developer temperature. Since a linear material reflects a linear response of image recording, a γ-value close to 1 is desired. If the temperature is too low, however, the development speed becomes also very low. In this case, the development time must be increased to compensate for it. However, long development times give rise to the lift-off problem. A compromise is found at a temperature of 9°C. The scattering level remains low at 9°C and the γ-value only increases to 1.2.

With the developer temperature of 9°C, the same experiment as that shown in Fig. IV.16. was performed. The result is given in Fig. IV.18. The roughness at low temperatures looks much better than that at room temperatures. The dilution ratio of 2:1 at low temperatures also shows reduced roughness, if compared with the 1:1 at room temperature. The worst roughness value from 2:1 dilution ratio is 10.2nm and that from 1:1 is 7.3nm. These two values are found for ET1 and DT=25". This is a significant improvement compared to the result shown in Fig. IV.16.

At the developer temperature of 9°C, the influence of the development time ranging from 5s-30s and developer dilution ratios from 1:1 to pure are shown in Fig. IV.19. The scattering level is low for short development times and for the most diluted developer. With this process, even the relative scattering level of 0.4-0.6 in the legend box of Fig. IV.19. is improved over that obtained with 1:1 dilution at the room temperature. Further experiments are also carried out for higher dilutions like 1:2. But development times longer than 60s are needed to develop the unexposed area. With such long development times, swelling and lift-off problems are observed.

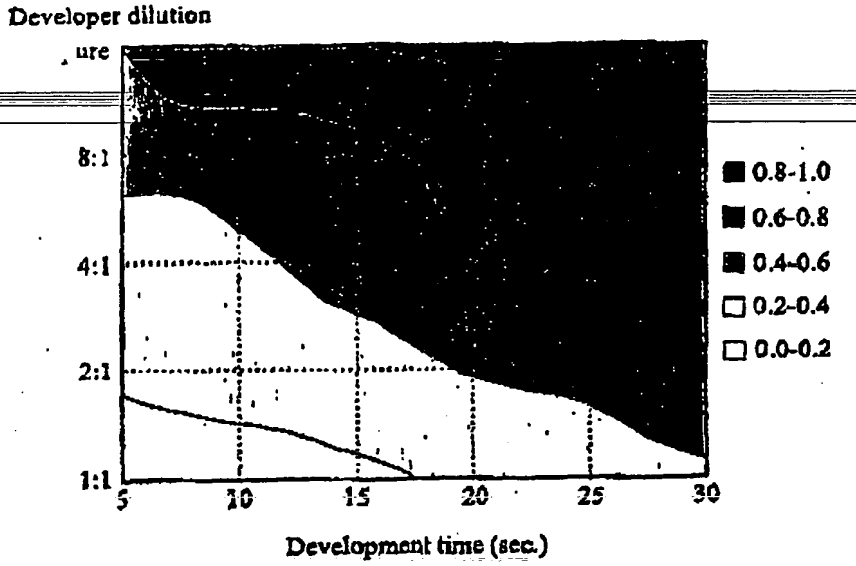

Fig. IV.19. Scattering distribution as a function of development time and developer dilution ratio at the developer temperature of 9°C.

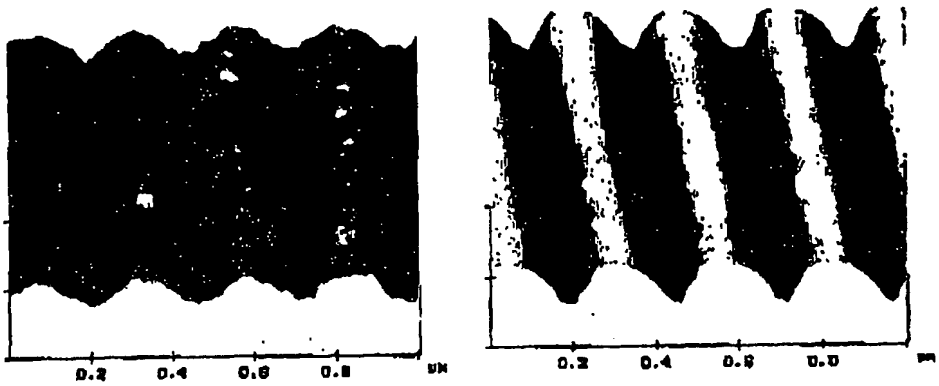

a) b)

Fig. IV.20. Surface roughness comparison between a) the harsh and b) the mild processes.

AFM scanned images for the gratings made by the TIR holography are shown in Fig.IV.20. for the case of the harsh and the mild processes. The process conditions for the harsh and the mild processes

are pure developer at 23°C and 1:1 dilution at 9°C, respectively. The mild process shows much smoother surface quality than that of the harsh process.

IV.3. Summary

Many contributing factors to the scattering intensity are investigated such as the prebake temperature, the prebake acceleration time, the resist thickness, the dilution ratio, the chuck type, the developer concentration, the development time, and the developer temperature.

It is useful to quantify the influence of each factor towards the total scattering intensity. Only relative values of the scattering intensities are presented for previous figures (Fig. IV.4-8, 10, 13, 19). Our raw data are used for the calculation of the scattering contribution of each factor. Multiple times (~5 times) of experiments were carried out for each figure to verify the reproducibility. Average values are used for the calculation.

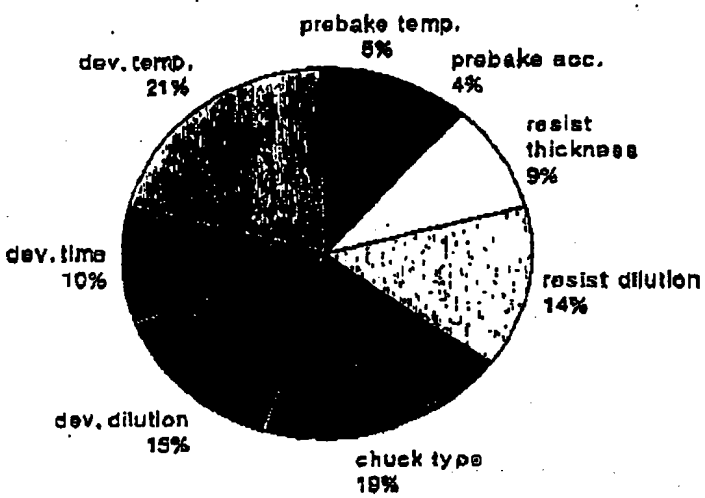

Fig. IV.21. The influence of each factor on scattering suppression.

Figure IV.21. summarises the contribution of each factor. The four most important factors are the developer temperature, the chuck type, the developer dilution, and the resist dilution. These four factors occupy ~70% of the contribution to reduce the total scattering. Since the effect of the chuck type and that of the resist dilution are closely coupled, the effect of the resist dilution can be nested within the effect of the chuck type. In that case, the volume effect (prebake temperature and acceleration, thickness, and chuck type) corresponds to 40%, while the surface effect corresponds to 60%. None of the factors in Fig. IV.21. is negligible. Therefore, to improve the scattering significantly, all these factors should be optimised to suppress the scattering. With proper optimisation, scattering intensity can be reduced by a factor of ~10.

The optimised process conditions are summarised in Table. IV.1.

Items	Conditions
Resist thickness	250nm
Prebake temperature	130°C
Prebake acceleration	130°C per 5 minutes
Resist dilution ratio	undiluted
Type of chuck	closed chuck
Developer dilution	1:1 (MF322:water)
Development time	15s
Developer temperature	9°C

Table. IV.1. Optimised process conditions of SNR240 for scattering suppression.

References

1. R.R.A. Syms, *Practical Volume Holography*, 344 (1990), Clarendon express, Oxford.
2. H.J. Bjelkhagen, *Silver halide recording materials for holography and their processing*, Springer Series in Optical Sciences, 66, Springer Verlag (1963).
3. W. Gladden, R.D. Leighty, "Recording media" in *Handbook of Optical holography*, H.J. Caulfield, Ed., 227-298, Academic Press, New York (1979).

VI. Hologram image transfer into fused silica substrate

The relief image in resist has a lot of problems in actual application[1]. Problems of the resist-relief image as a hologram are: i) the characteristics (transmittance, groove depth and profile) of the resist material changes over time and illumination dose. ii) the resist is mechanically weak (i.e., against scratches). iii) the resist hologram is difficult to clean. To avoid such problems, it is suggested that the relief image be transferred into its substrate. The advantages of the etched relief hologram are the opposite of those problems that the resist hologram has. In addition, it is possible to improve the diffraction efficiency by increasing the surface modulation depth. The noise level may also be decreased by smoothening the surface roughness.

Since the grating period is very short (242.8nm), it is difficult to obtain a good modulation depth with any wet etching technique that tends to have an isotropic etch behaviour. A dry etching technique is more appropriate, because anisotropic or isotropic etching characteristics can be achieved[2].

The dry etching condition should satisfy the requirement that the etch selectivity between the fused silica substrate and the resist be >1.2. The surface must also be free from polymers after the etching. Since the refractive index ratio between the resist (n=1.8) and the fused silica substrate (n=1.5) is 1.2, the etch selectivity between these two materials must exceed their index ratio to have a diffraction efficiency equal to or higher than that before etching. If an increased efficiency is desired, a multi-layer process is worth trying. In this chapter, we explore the etching process to improve the S/N ratio.

VI.1. Instability of resist hologram

Generally, the resist is composed of a base polymer, a photo-active compound, and a solvent[3,4]. In addition to them, SNR240 resist has a cross-linker that allows the exposed part of the resist to be cross-linked after post-exposure baking (PEB)[5]. But such a chemical reaction might be subjected to the high photon or thermal energy by DUV or >150°C. With such a high energy, all the components completely cross-link with each other, hence the absorption increases. With such a strong absorption, the

diffraction efficiency might be reduced accordingly. The relief image in resist can be changed by DUV irradiation which later gives rise to changed efficiency.

The SNR240 resist with a 250nm thickness is coated on a fused silica substrate. An absorber plate (BK7) is attached to the back of the fused silica substrate with a matching liquid in-between. This sample is recorded with an inter-beam angle of 60° using the transmission holographic set-up as shown in Fig. II.1. The grating period is 257nm which is the same as the wavelength of the laser. The grating profile is symmetric about the normal to the substrate. The diffraction efficiency is measured at the first Bragg angle (30°). The diffraction efficiencies of the 0^{th} and the 1^{st} transmitted orders are measured at $100mW/cm^2$ for one hour. The total exposure dose that the grating receives for one hour is $360J/cm^2$. Figure VI.1. shows the results. The initial diffraction efficiencies for the 0^{th} and the 1^{st} orders are 36.5% and 13.5%, respectively. With an increasing exposure time, both of the efficiencies decrease. The efficiencies for the 0^{th} and the 1^{st} orders decrease by 38% and 26%, respectively during one hour. The efficiencies for the reflected orders slightly increase by ~5%. If there is no absorption, the sum of all orders should remain constant. If the diffraction efficiency for the 0^{th} order decreases, that for the 1^{st} order should increase. But in this figure, the two decrease simultaneously. This is interpreted that the absorption is the major cause of the efficiency drop. The grating profile must also be changed slightly judging from the diffraction efficiencies increases for the reflected orders. Accordingly, the DUV irradiation modifies the resist profiles.

If an efficiency decrease of only 10% is allowed for the 1^{st} order to guarantee a reproducible process, only 15 minutes of exposure time can be tolerated with a light intensity of $0.1W/cm^2$. This corresponds to an exposure dose of $90J/cm^2$. If a surface relief grating recorded with the TIR holographic set-up is considered, the diffraction efficiency will be ~5% using the optimised process. Because of this low diffraction efficiency, the exposure time should be increased for reconstruction. It is worthwhile to see how many exposure events can occur with the tolerable exposure dose of $90J/cm^2$. The number of allowable exposure events, N, is estimated by

$$N = \frac{E_{ml}\eta}{E_p}, \qquad \text{(VI.1)}$$

where E_{tol} and E_p are the tolerable exposure dose and the exposure dose necessary for printing, respectively, and η is the diffraction efficiency of the grating. If the necessary exposure dose for printing is assumed to be 50mJ/cm^2, the number of allowable exposure events will be <90. Because the number of the integrated circuit (IC) chips per wafer is ~150, which is typical for memory chips, the resist hologram cannot be used even for one wafer. Therefore, the resist hologram is not useful for mass-production of IC chips.

In addition to the efficiency drop, we have also observed a reduction of the scattering with the DUV irradiation. A specimen with plenty of graininess referred to as "pop-corns" is exposed to the DUV for 10 J/cm^2. The scattering diminishes considerably. Figure VI.2. shows the AFM-scanned images before and after DUV irradiation. All the pop-corns disappeared after the DUV cure with 10 J/cm^2. These pop-corns are known to be a round gaseous residues[6]. The pop-corns explode or the gas within the envelops leaks away during DUV curing. Such pop-corns are often formed with old resists. The shelf life of the resist is six months. A lot of pop-corns are observed with the resist older than six months. Therefore, the pop-corns are not common as long as the resist is used within the shelf life. But the DUV cure is worth employing to minimise the surface roughness before etching.

With the DUV cure at 10J/cm^2, the resist profile and the modulation depth remain unchanged. But the diffraction efficiency is slightly decreased presumably due to the increased absorption.

VI.2. Enhancement of S/N ratio

Besides the hologram stability, the etched hologram also permits us to enhance the S/N ratio by both enhancing the etching depth and reducing the number and the size of the scattering centres. If the modulation depth within the resist hologram is sufficiently deep, it is not very difficult to obtain deep grooves in fused silica substrate. If we choose a proper etch selectivity between the substrate and the resist, we can smoothen the surface without deteriorating short period gratings. In this way, it is possible to enhance the S/N ratio.

To satisfy the above requirements, a good etching condition must be established. The processing condition has to be established to achieve a reasonably high etch selectivity, enough to obtain a deep etch groove and to smooth the etched surface. We found the best etching condition with our dry etching system, a GIR300 Alcatel:

Gas mixture ratio	: H_2:CF_4/O_2=3:10
Chamber pressure	: 3 mTorr
RF power	: 5 W for the 1st 10% etching and 40 W for the rest.
DC bias	: 380V
Etching time	: varied depending on the necessary etch depth

Table VI.1. Optimised etching process conditions.

Apart from the pop-corns that can be eliminated by DUV cure, there are fine grains on the hologram gratings. These grains should be reduced in size before etching the fused silica substrate. The general grain size is smaller than the grating features and they are also spatially separated from each other. If we employ a poorly selective etching condition, it is possible to attack the grain more effectively than the grating.

Figure VI.3. indicates how the grain size is reduced during etching. Since the etch species attack the resist as well as the substrate in a 3-dimensional fashion, the accessability of the species to the grain is higher than that of the grating structure. Therefore, the grain is eroded faster than the wanted feature. This leaves small and shallow etched grains behind as schematically shown in Fig. VI.3.d). The scattering flux density is directly proportional to the 6th power of the diameter of the scattering centre[7-12], while the diffraction efficiency is increased with depth. Therefore, it is more effective to reduce the size of the grain than to reduce the scattering level.

It is also stressed that the etch rate should carefully be controlled to guarantee smooth surfaces. If the ion energy of the plasma is very high, the energetic ions might generate rough surfaces on the resist gratings, which can again be transfetred to the substrate. In this case, the groove depth cannot be homogeneous over the grating area due to random attacks of the resist and the substrate. In practice, an S/N ratio of <1 is observed with a DC bias > 400V. This is as a result of decreased etching depth and

increased surface roughness. Therefore, slow and gentle etching is required. We tuned the etching process such that smooth surfaces are produced for an etch rate of ~10nm per minute.

Fig. VI.3. Etching model for a) a systematic structure and b) a particle. The accessability of the etching radicals for a particle is higher than that for a systematic structure. The relative size reduction of the particle after etching is considerably bigger than that of the desired structure.

VI.2.1. Experiment and discussion

An experiment is performed to prove that scattering reduction is possible with etching. A resist hologram with some grains is prepared for the etching. This hologram undergoes the first etching step with a low selectivity etching for smoothening the roughness. For the second step, higher etch selectivity is desired than in the first step.

Since our best selectivity between the fused silica substrate and the resist is 2.85, it is barely possible to obtain a groove depth in SiO_2 of ~140nm using resist gratings with 50nm depth. For this experiment, however, we use an etch selectivity of 1.5 to improve the surface roughness.

An AFM is used to show the profiles of the resist and fused silica gratings in Fig. VI.4. A fraction of the gratings are used that are recorded with a knife-edge mask. If a scanning electron microscope (SEM) is used, coating with gold or carbon is needed to prevent charging effects that blur the image. With coatings, new grains caused by the deposited conducting materials can also be formed that disturb the original surface details (see Fig. III.4). It is apparent that the surface of the fused silica grating is almost free of grains compared with the resist grating.

With these gratings, we measure the signal and the noise. Figure VI.5. shows the result. The noise decreases by a factor of 3, while the signal remains the same. The signal to noise ratio with the resist hologram is 3.5 and that with the fused silica substrate becomes 8.1, which is improved by a factor of 2.3. We concluded that the etching is more effective to reduce the noise than to increase the signal.

Fig. VI.4. Roughness comparison between resist and fused silica holograms.
a) Resist hologram with grains. b) Fused silica hologram etched using the resist hologram of a).

VI.3. Enhancement of diffraction efficiency

A high diffraction efficiency is required for a high productivity, if the holographic technology is to be implemented as an exposure tool. Since TIR holography uses only one prism as a primary optics, the machine can be made small in size. However, if the diffraction efficiency remains low, the laser power must be increased instead. This requires a huge laser or multiple combined lasers to enhance the throughput. Thus a small machine with a huge light source might result. To keep the whole machine small and to save expensive cleanroom space, enhancing the efficiency is the best solution. Since the diffraction efficiency before etching is only ~5%, the throughput must be lower than that of conventional steppers. With this low efficiency, the advantage of this technology is diluted.

Since the surface modulation depth of the resist hologram is shallow for an etch mask, it is difficult to increase the modulation depth enough for high efficiency. One way to enhance the diffraction efficiency is to employ a multi-layer process in spite of its complexity[13-16].

VI.3.1. Experiment and discussion

Figure VI.6. illustrates two different methods to transfer the surface-relief hologram into the substrate. One is a direct etching (Fig. VI.6.a)) and the other is the multi-layer process (Fig. VI.6.b)). For a deep modulation depth, the latter is used.

The first step for this process is to deposit a thin film that is resistant against etch radicals on the resist hologram. For our experiment, we use silicon-mono-oxide (SiO) that can be easily deposited in a conventional evaporator. The thickness of SiO is ~50nm. Then a resist layer is spin-coated on the SiO film. The resist thickness is sufficiently high that the top surface of the resist becomes flat. We use a 300nm thick resist for this. This resist is etched back using oxygen (O_2) until the top features of the SiO is exposed. A further etch-back is performed with a 1:1 etch selectivity between the resist and the SiO until the crest of the SiO layer is removed. Because of the shallow modulation depth, the slow etch rate must be precisely controlled. If the etch-back is finished, the crest of the bottom resist or the resist hologram is exposed, while the SiO layer remains in the trough. The SiO layer in the trough plays the role of an etch mask during the etching of the bottom layer resist. Once the resist is etched, the silica substrate undergoes the main etching, with which the deep permanent grating is produced. With this process, a reversed tone results. This reversed tone is not a problem as long as the grating period is maintained. Because the tone is already reversed during recording using a negative photoresist of SNR240, another tone-reversal after etching gives a positive tone. Cross-sectional SEM micrographs corresponding to Fig. VI.6. are shown in the appendix A.2.

The diffraction efficiency is calculated for the etched grating. The coupled wave theory is used for this calculation[17]. The etched grating is placed on the prism with a matching liquid in-between and illuminated with the conjugated reference beam. The 1st order transmitted beam is measured for five different grating depths. Figure VI.7.a) shows the result. The grating profile that is used for the calculation and measurement is shown in Fig. VI.7.b).

The diffraction efficiency increases with increasing grating depth until the depth reaches 180nm. The measurement result is in good agreement with the results of the calculation. The highest efficiency of 37% is found at the depth of 180nm. A large range of 160nm-220nm depths gives efficiencies of >35%. This means that non-uniform etching is not a problem.

With the direct etching technique, it is difficult to obtain a deep groove because of the shallow modulation depth in the resist. The depth that can be obtained with the process conditions shown in Table. VI.1. is in the range of 50nm-80nm that corresponds to 10%-17.5%. It is also difficult to obtain a good homogeneity across the exposure field, because the diffraction efficiency changes a lot with etch

depth variation. With the multi-layer process, on the other hand, it is easy to obtain deep grooves up to ~500nm. Therefore, it is even easier to obtain a 180nm deep grating for the highest diffraction efficiency.

With the multi-layer process, scattering is significantly reduced. The roughness on the grating is covered twice by the SiO layer and the top resist layer. During the etch-back and the main etching step, the resulting roughness is weakened.

VI.4. Summary

The surface-relief image in resist shows that the diffraction efficiency degrades over time. Once this image is transferred in the SiO_2 substrate, not only this problem but others also are improved. Among the improved performances are : i) mechanical robustness, ii) reduced scattering , and iii) high diffraction efficiency.

The etched gratings can be cleaned in a boiling sulfuric acid bath. This is never possible with resist gratings due to fast solubility in this acid. The etched gratings are resistant against scratching. No diffraction efficiency degradation is observed during an exposure dose of ~1000J/cm^2 on our selected SiO_2 substrate. No color center is observed with this energy yet. An increased exposure dose is not expected to degrade the diffraction efficiency.

With the direct etching technique, we obtain ~15% diffraction efficiency which is far higher than that obtained with a resist hologram. A multi-layer process gives ~35% diffraction efficiency with a large etch depth latitude of 160nm-220nm.

Scattering level is reduced by etching regardless of the etching process employed.

References

1. Rolf C. Enger Steven K. Case, "Optical elements with ultrahigh spatial-frequency surface corrugation", *Appl. Opt.*, 22(20), 3220-3228, Oct. (1983).
2. David J. Elliott, *INTEGRATED CIRCUIT FABRICATION TECHNOLOGY*, 259 (1982), The Kingsport Press.
3. David J. Elliott, *INTEGRATED CIRCUIT FABRICATION TECHNOLOGY*, 167 (1982), The Kingsport Press.
4. L.F. Tompson, C.G. Willson, and M.J. Bowden, *Introduction to Microlithography*, ACS Symposium series 219, 111-116 (1983), American Chemical Society, Washington, D.C.
5. John Sturtevant, Steve Holmes, and Paul Rabidoux, "Post-exposure bake characteristics of a chemically amplified deep-ultraviolet resist", *SPIE*, 1672, 114-124 (1992).
6. Private talk with Dr. C.G. Park of Shipley Co., Japan, (1998).
7. R.R.A. Syms, *Practical Volume Holography*, 138 (1990), Clarendon express, Oxford.
8. L. Solymar and D.J. Cooke, *Volume Holography and Volume grating*, 262 (1981), Academic press.
9. R.S. Longhurst, *Geometrical and Physical Optics*, 494, Longman, London (1986).
10. P. Hariharan, *Optical holography*, 102, Cambridge University Press (1996).
11. P. Hariharan, G.S. Kaushik, and C.S. Ramathan, "Reduction of scattering in photographic phase holograms", *Opt. Commun.*, 5(1), 59-61, April (1972).
12. P. Hariharan, "Simplified, Low-noise processing technique for photographic phase holograms", *Opt. Commun.*, 6(1), 75-76, Sept. (1972).
13. L.F. Tompson, C.G. Willson, and M.J. Bowden, *Introduction to Microlithography*, ACS Symposium series 219, 288-293 (1983), American Chemical Society, Washington, D.C.
14. Woo-Sung Han, *PHOTOLITHOGRAPHY*, 132-133 (1992), Samsung Training Center, Kihung.
15. David S. Soane and Zoya Martynenko, *Polymers in Microelectronics*, 132-139 (1989), Elsevier, Amsterdam.
16. Ralph Dammel, *Diazonaphtoquinone-based Resists*, 136-149 (1990), SPIE Optical Engineering Press, Bellingham, Washington, USA.
17. M.G. Moharam and T.K. Gaylord, "Diffraction analysis of dielectric surface-relief gratings", *J. Opt. Soc. Am.*, 72(10), 1385-11392, Oct. (1982).

Claims:

1. ~~Method of forming a hologram from a information containing~~ mask, comprising the following steps:
- arranging a substrate bearing a layer of a holographic recording medium on a first face of a coupling element and in optical contact therewith;
- arranging a information containing mask in a spaced relationship and parallel to the substrate;
- generating an illumination light beam and then splitting the light beam into an object beam and a reference beam;
- directing the reference beam to a second face of the coupling element in a way that the condition for total internal reflection at the interface between the recording medium and the ambient medium is fulfilled;
- directing the object beam through the mask to the substrate such that it coincides with the reference beam in the holographic recording medium;
further including the steps of
- employing a photoresist as the holographic recording medium; and
- arranging the planes of polarisation of the object and reference beams incident on the holographic recording medium such that their polarisation vectors are substantially mutually orthogonal in the holographic recording medium and such that the polarisation vectors of the incident and totally internally reflected reference beams are also substantially orthogonal.

2. Method according to claim 1, characterized in that only the transmission hologram is recorded in the holographic recording layer.

3. Method according to claim 1 or 2, characterized in that the plane of polarisation of the object beam is at 45° to

the plane of incidence of the reference beam at the holographic recording layer.

4. Method according to any of claims 1 to 3, characterized in that the object beam illuminates the mask at an off-axis angle i.e. not normal to the mask.

5. Method according to any of claims 1 to 4, characterized in that the photoresist material is selected such that its thickness (d) and absorption (a) meet the condition $a * d < 1$.

6. Method according to any of claims 1 to 5, characterized in that the photoresist is selected such that its contrast described by its gamma-value satisfies the condition $\gamma < 3$.

7. Method according to any of claims 1 to 6, characterized in the photoresist is selected such that its resolution described by the smallest period of grating that can be optically recorded in the material is with a modulation depth $(d_{max} - d_{min}) / (d_{max} - d_{min}) > 25\%$ satisfies the condition $\Lambda < 200$ nm.

8. Method according to any of claims 1 to 7, characterized in that laser light of a wavelength below 300nm, and preferably of a wavelength between 150 and 260 nm for recording the hologram is used.

9. Method according to any of claims 1 to 8, characterized in the polarisation angles are selected according to the refractive index of the photoresist.

10. Method according to any of claims 1 to 9, characterized in that a combination of polarisation angles of between 37 to 44°, preferably 39° for the reference beam and - -43 to

-47°, preferably -45° for the object beam with respect to the plane of incidence are applied.

11. Method according to any of claims 1 to 10, characterized in that the intensity of the reference beam exceeds that of the object beam.

12. Method according to any of claims 1 to 11, characterized in that the intensity of the reference beam exceeds that of the object beam by a factor 2, and preferably is 4 : 1.

13. Method according to any of claims 1 to 12, characterized in that the intensity ratio of the object and reference beams is between 3:1 and 5:1, and preferably about 4:1.

14. Method according to any of claims 1 to 13, characterized in that the thickness of the photoresist layer is less than 500 nm, preferably between 100 and 300 nm and most preferably between 200 and 300 nm.

15. Method according to any of claims 1 to 14, characterized in that the image recorded in the photoresist as surface relief hologram is transferred into the substrate material by an etching process.

16. Method according to any of claims 1 to 15, characterized in that the etching process is a plasma etching process.

17. Method according to any of claims 1 to 16, characterized in that the illumination beam (51) is scanned in a first direction across the holographic recording medium (79) and the mask (73), respectively , stepping the illumination (51) beam in a second direction perpendicular to the first dir ction, and then scanning the beam (51) again in the first direction and so on, such that the

reference and object beams (75,74) travel simultaneously across the first face or the substrate (77) in optical contact with the first face;

18. Method according to any of the preceding claims 1 to 17 characterized in that the gap between the holographic recording layer and the mask is determined, e.g. interferometrically, and then the distance between the hologram and the recording medium adjusted to a predetermined value.

19. Method according to any of the preceding claims 1 to 18 characterized in that in the hologram reconstruction process the distance between the hologram and the substrate onto which the holographically recorded image is to be reconstructed is adjusted to the value as maintained between the holographic recording layer and the mask in the hologram formation process.

20. Use of the method according to any of claims 1 to 19 for recording features of less than 1 µm, preferably less than 0.5 µm, contained in a mask in a hologram for use in microlithography.

21. Total internal reflection holographic recording apparatus for recording a hologram from a mask, comprising
- an optical coupling element for receiving a substrate on a first face;
- a substrate bearing a holographic recording medium, the substrate being in optical contact with said first face of the optical coupling element,
- at least one light source for generating a light beam;
- optical means for generating a collimated light beam of a selected cross-section;

- means, e.g. a beam-splitter, prism or the like, for generating two coherent light beams, a reference light beam and an object light beam;
- means for directing the reference light beam at a second face of the coupling element such that it illuminates the interface between the first face and the ambient medium or the interface between a substrate in optical contact with said first face and the ambient medium at an angle greater than the critical angle;
- means for directing the object light beam at the first face of the coupling element such that it is aligned with the reference beam in the plane of the holographic recording medium on the substrate in contact with the first face;

characterized in that

- the holographic recording medium is a photoresist; and
- means are provided for arranging the planes of polarisation of the object and reference beams incident on the holographic recording medium such that their polarisation vectors are substantially mutually orthogonal in the holographic recording medium and such that the polarisation vectors of the incident and totally internally reflected reference beams are substantially orthogonal.

22. Apparatus according to claim 21 characterized in that the at least one light source is a laser light source emitting light of a wavelength below 300nm, and preferably of a wavelength between about 150 and 260 nm; and preferably between about 190 and 254 nm.

23. Apparatus according to claim 21 or 22, characterized in that the photoresist material is such that its thickness (d) and absorption (a) meet th condition a * d < 1.

24. Apparatus according to any of claims 21 to 23, characterized in that the photoresist material is such that that its contrast described by its gamma factor satisfies the condition $\gamma < 3$.

25. Apparatus according to any of claims 21 to 24, characterized in that a combination of polarisation angles of between 37 to 44°, preferably 39° for the reference beam and - 43 to -47°, preferably 45° for the object beam are applied.

26. Apparatus according to any of claims 21 to 25, characterized in that means are provided for adjusting the intensities of the object and reference beams such that the intensity of the object beam exceeds that of the reference beam.

27. Apparatus according to any of claims 21 to 26, characterized in that the intensity of the object beam exceeds that of the reference beam by at least of a factor 2 preferably by a factor of about 4.

28. Apparatus according to any of claims 21 to 27, characterized in that the thickness of the photoresist layer is less than 500 nm, preferably between 100 and 300 nm and most preferably between 200 and 300 nm.

29. Apparatus according to any of claims 21 to 28, characterized in that means are provided for scanning and stepping the incident light beam in a raster scan across the beam splitting means in a first and in a second direction, respectively, such that the reference and object beams travel simultaneously across the first face or the substrate in optical contact with the first face;

30. Apparatus according to any of the preceding claims 21 to 29 further comprising

- means for measuring the gap between the hologram and a wafer being arranged in a spaced relationship to the hologram; and
- means for adjusting the parallelism and/or separation between the hologram and the wafer.

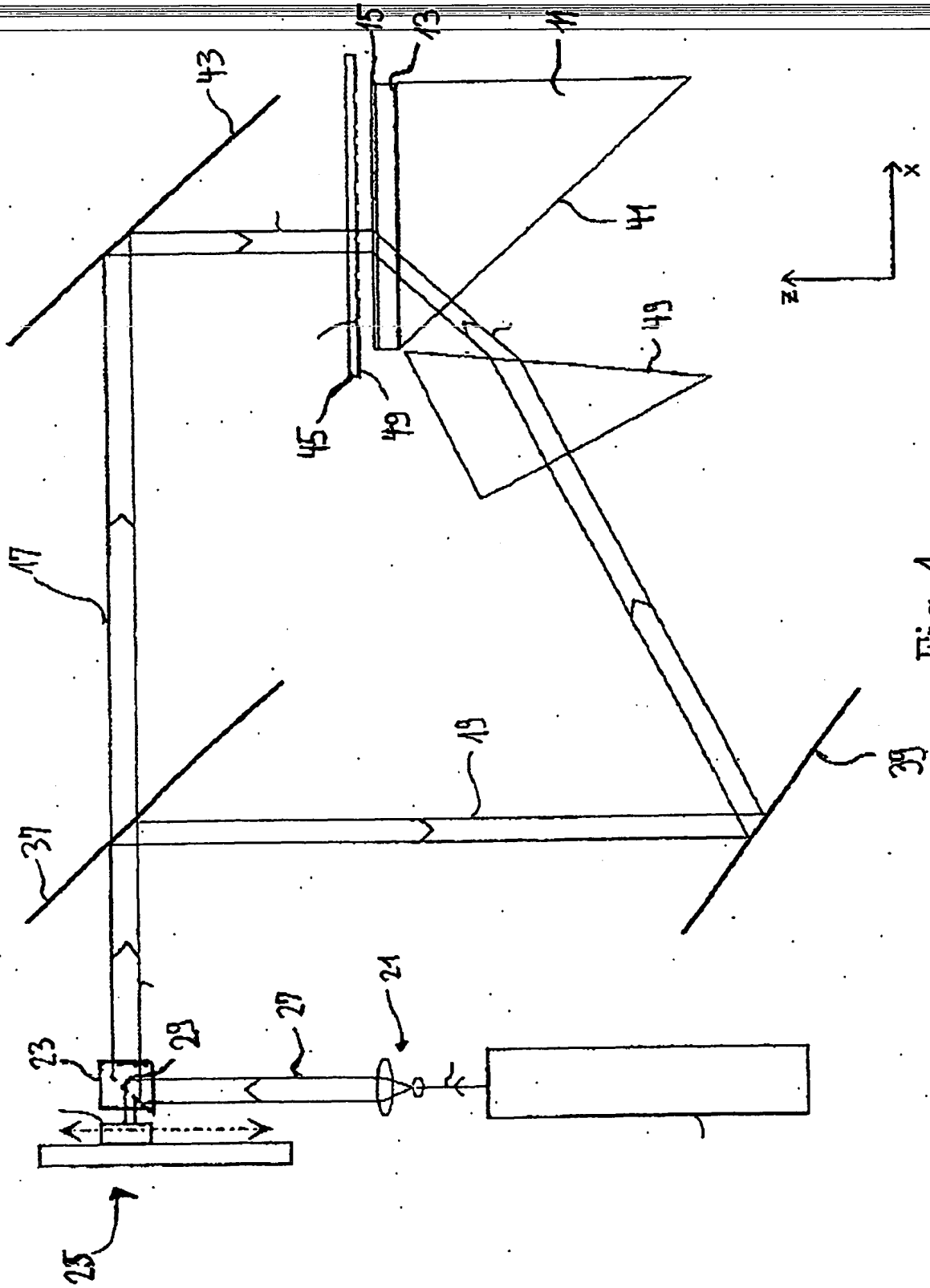

Fig. 1

Fig. 2

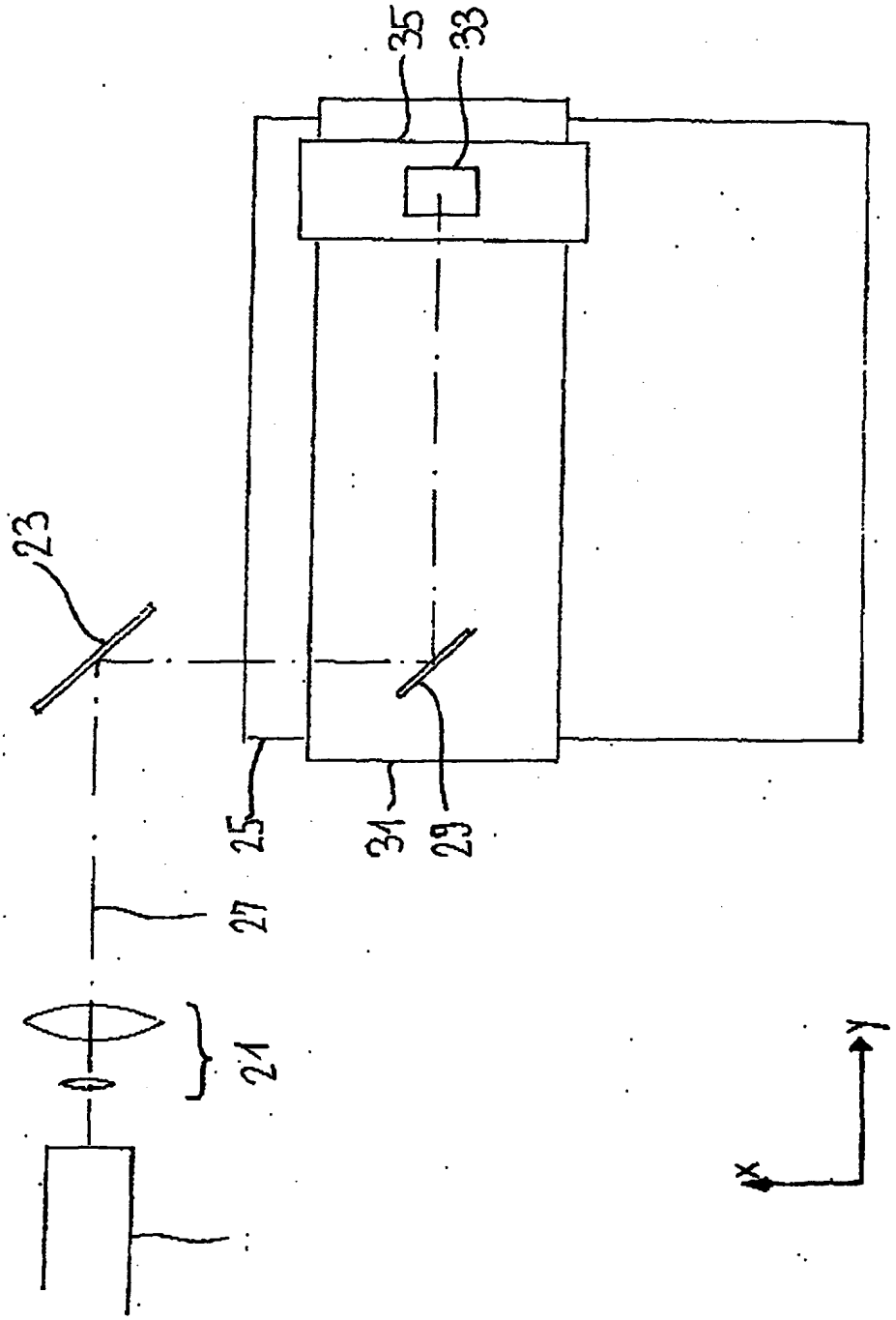

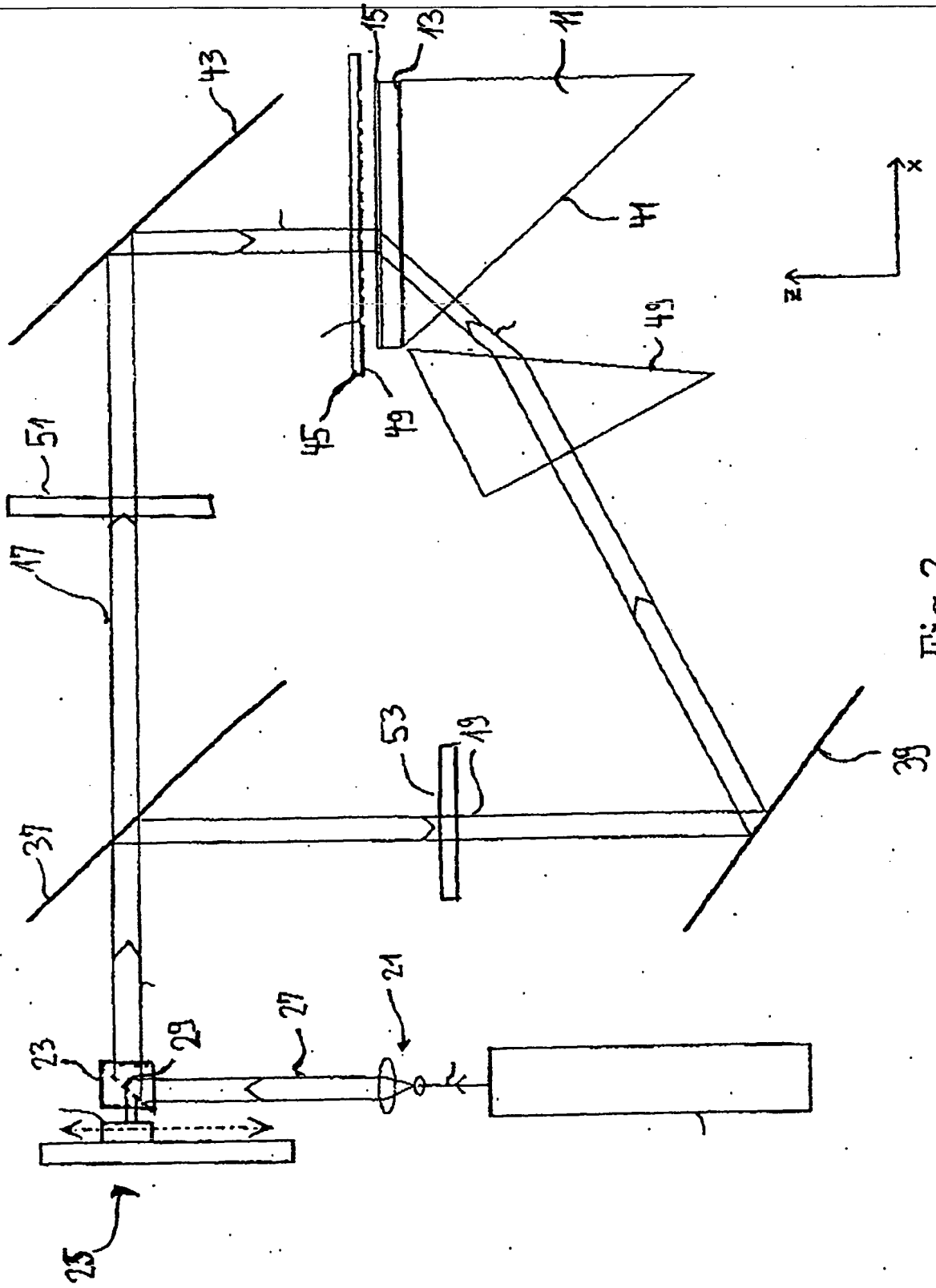

Fig.3

Abstract

The present invention relates to a method and an apparatus for forming a hologram from a mask. According to the invention a photoresist is used as the holographic recording medium and the planes of polarisation of the object and reference beams incident on the holographic recording medium are arranged such that their polarisation vectors are substantially mutually orthogonal in the holographic recording medium and such that the polarisation vectors of the incident and totally internally reflected reference beams are also substantially orthogonal. Preferably, just the transmission is formed in the holographic recording layer.

(Fig. 3)